의학박사 학위논문

# FTY720 effects on Alzheimer's disease mouse brain revealed by spatial transcriptomics

공간 전사체학으로 밝힌

FTY720의 알츠하이머병 쥐의 뇌에 미치는 영향

2022년 08월

서울대학교 융합과학기술대학원

분자의학 및 바이오제약학과

서 훈 녕

# FTY720 effects on Alzheimer's disease mouse brain revealed by spatial transcriptomics

지도 교수 이 동 수

이 논문을 의학박사 학위논문으로 제출함
2022년 4월

서울대학교 융합과학기술대학원
분자의학 및 바이오제약학과
서 훈 녕

서훈녕의 의학박사 학위논문을 인준함
2022년 7월

위 원 장 _____ 이 형 기 _____ (인)

부위원장 _____ 이 동 수 _____ (인)

위 원 _____ 구 자 욱 _____ (인)

위 원 _____ 신 영 기 _____ (인)

위 원 _____ 이 윤 상 _____ (인)

# ABSTRACT

# FTY720 effects on Alzheimer's disease mouse brain revealed by spatial transcriptomics

Hoon Young Suh

Department of Molecular Medicine and Biopharmaceutical Science,

The Graduate School of Convergence Science and Technology,

Seoul National University

Since there is a need for faster application of neurodegenerative drugs in the clinical field, finding new indications for already approved drugs gained attention. FTY720 (fingolimod) is an FDA-approved drug for Multiple sclerosis, and its application to Alzheimer's disease (AD) is promising. Recent studies, however, lack a comprehensive analysis of the CNS effect of FTY720 considering regional and cellular diversities of the brain.

In this study, spatial transcriptomic data from 7-month-old mice with orally administered FTY720 at a dose of 0.3 mg/kg/day for 7 weeks

was analyzed. In the Y-maze test, poor behavior with 5xFAD AD model mice was recovered by FTY720. The deposition of amyloid beta was increased in 5xFAD, but remained unchanged by FTY720. S1PRs, the target receptor of FTY720, showed distinct spatial patterns in the WM. In addition, weighted gene co-expression network analysis (WGCNA) modules localized in the WM and cortex were correlated with oligodendrocyte and neurons, respectively.

Integrative analysis of spatial transcriptomic data and public single-cell data by Necessary and Sufficient Forest (NS-Forest) and CellDART was performed to evaluate the spatial distribution of brain cells. FTY720 induced transcription of myelin-forming oligodendrocytes in the WM of 5xFAD. Glutamatergic neurons and GM-associated astrocytes in the cortex showed an increased pattern in 5xFAD, while FTY720 reversed their transcriptomic profile. The increased pattern of dopaminergic neurons in the ventral tegmental area by FTY720 was observed in 5xFAD. Myelin-forming oligodendrocytes in the WM, glutamatergic neurons and GM-associated astrocytes in the cortex were associated with the behavior change.

Oral FTY720 induced transcriptional change to the target receptor S1PRs in the WM along with the upregulation of myelin-forming oligodendrocyte in the WM. Besides, glutamatergic neurons and

GM-associated astrocytes in the cortex shared similar transcriptional patterns according to FTY720. In summary, FTY720 might directly act on the myelin-forming oligodendrocytes in the WM through S1PRs, resulting in the transcriptional regulation of glutamatergic neurons and GM-associated astrocytes that cause behavioral changes. Area-specific cell subtypes that contributed to the behavioral change by FTY720 were found in 5xFAD. The spatial transcriptome changed by FTY720 in 5xFAD AD model mice was similar to the spatial transcriptome in normal mice, which is thought to have shown the potential of FTY720 as a treatment for AD. Moreover, these results help to understand the area-specific and cell-specific effects of FTY720. Comprehensive analysis of spatial transcriptome and single-cell data can be applied to confirm the regional and cellular effects of other CNS-targeted drugs.

**Keywords:** FTY720; brain; drug effect; spatial transcriptome; single-cell sequencing; cell composition; spatial distribution

***Student Number:*** 2019-30531

# CONTENTS

# List of Figures

# List of Tables

# 1. Introduction

## 1.1 Drugs for Neurodegenerative diseases

Neurodegenerative diseases including Alzheimer's disease (AD), Multiple sclerosis (MS), and Parkinson's disease (PD) are the age-related incurable conditions that result in progressive degeneration of neurons in the central nervous system (CNS). Difficulty in the selection of disease target, the drug development for neurodegenerative disease thus far largely failed. Therefore, there is a great need to expand interest in target selection for neurodegenerative diseases.

### 1.1.1 Drugs for Alzheimer's disease

AD is a progressive neurodegenerative disease that accompanies a gradual decline in cognition. As the most common type of dementia [1], AD has become a target for disease-modifying drug development. Up to date, five drugs are approved by the U.S. Food and Drug Administration (FDA) for symptomatic AD [2]: donepezil, galantamine, memantine, rivastigmine, and donepezil and memantine. The histopathological hallmarks of AD are extracellular amyloid plaques and intracellular neurofibrillary tangles that result in neurotoxicity [3]. The molecular mechanisms involved in the pathogenesis of AD include APP mutation,

ApoE allele, overproduction and/or reduced clearance of amyloid beta, abnormal tau protein, oxidative stress, neuroinflammation, and alteration of lipid metabolism.

### 1.1.2 Strategy for drug development

Computational drug repurposing, or the *in silico* screening of FDA-approved drugs for new indications, is an emerging method for faster clinical application of drugs targeting neurodegenerative diseases [4, 5]. Traditional drug development is costly and time-consuming from bench to bed. However, recent advances in molecular-based drug repurposing include multi-omics data for predicting drug use [6]. These omics-based approaches are promising in drug development for neurodegenerative diseases such as AD or Multiple sclerosis (MS) that have unclear etiology.

## 1.2 FTY720 as a drug for Alzheimer's disease

### 1.2.1 Mechanism of FTY720

FTY720 (fingolimod) was approved as the first oral agent for relapsing-remitting MS by FDA since FTY720 has shown a significant effect on reducing relapse rate and inflammation on MRI [7, 8]. FTY720 is a structural analog of sphingosine that is generated by the ceramide

pathway. As a metabolite of the cell membrane constituent sphingomyelin, sphingosine and FTY720 are phosphorylated by sphingosine kinase to produce active S1P and FTY720-P. FTY720-P binds to sphingosine-1-phosphate receptors (S1PRs), S1P1, S1P3, S1P4, and S1P5 [9]. FTY720 induces S1PRs to internalize from cell membranes after binding [10]. Therefore, FTY720 acts as a functional antagonist at S1PRs to inhibit S1P-mediated cell signaling. The decrease of S1PRs activity in lymphocytes correlated with sequestration of lymphocytes in the lymph nodes [11]. The retention of central memory T lymphocytes reduced the infiltration of T lymphocytes to the CNS [12], thus preventing the local generation of effector T lymphocytes, abolishing astrogliosis, and stopping the recruitment of peripheral immune cells to the CNS [13].

### 1.2.2 Therapeutic potential of FTY720

The exposure of FTY720 to the central nervous system (CNS) after oral administration was shown in previous pharmacokinetic studies. Oral administration of FTY720 at 0.3 mg/kg resulted in high levels of FTY720-P level in the CSF [14]. As a result, the brain level of FTY720 was considerably higher than the blood level of FTY720 in experimental autoimmune encephalomyelitis (EAE) models as seen in normal rats [14,

15]. In addition, PET/CT studies using [14C]FTY720 in healthy mice confirmed its delivery to the brain, particularly to white matter (WM) [14, 16]. The co-localization of FTY720 with myelin suggests that the majority of FTY720 is integrated into myelin membranes. As a lipophilic molecule, FTY720 can cross the blood-brain barrier (BBB) and has been proven to exert direct effects on the CNS. SIPRs, targets for FTY720, are expressed on most brain cells, particularly neurons and glia [17]. *In vitro* and *in vivo* studies with FTY720 suggested the modulation of S1PRs in oligodendrocytes, neurons, astrocytes, and microglia [18-20]. As a result, FTY720 enhances myelination, protects neurons against excitotoxic insult, reduces reactive astrogliosis, and inhibits microglial activation [21].

The importance of sphingolipid metabolism in AD was suggested by laboratory and animal studies. Lipids are crucial to organizing the membrane of neurons and maintain cellular function. AD brain showed dysregulation of lipid metabolism that leads to the accumulation of proinflammatory ceramides and sphingomyelines [22, 23]. Moreover, emerging evidence support the efficacy of FTY720 in the brain of AD using 5xFAD AD model mice [24, 25]. Collectively, these data suggested that FTY720 may provide more benefit in the treatment of central inflammation in neurodegenerative disease, thus turning the focus of

drug development from autoimmune diseases to neurodegenerative diseases. However, there are limits to interpreting the CNS effect of FTY720 since these studies lack consideration of the region-specific changes and underlying cellular diversities in the brain.

### 1.3 The brain characteristics of Alzheimer's disease

#### 1.3.1 Susceptible areas in Alzheimer's disease

The hippocampus, a brain area important for memory and cognition, is vulnerable to damage in the early stages of AD [26]. The hippocampal circuit has been composed as trisynaptic excitatory pathway [27]. Evidence support that the preservation of hippocampal neurons has delayed AD-associated cognitive decline [28, 29].

Moreover, studies have implicated the abnormalities in the WM in the onset and progression of AD [30]. Histological researches demonstrate the degeneration of WM in AD [31, 32]. Independent with gray matter lesions, AD brain had axonal and oligodendroglial loss accompanied by gliosis in WM. However, the connection between WM changes and classically described AD pathology shown as hippocampal atrophy is still unknown. The regional patterns and potential mechanisms of WM pathology in AD are still unclear.

### 1.3.2 Major brain cells in Alzheimer's disease

Oligodendrocytes are myelinating cells that are essential for brain function. Oligodendrocytes continue to be produced in the adult brain in the ventricular area and migrate to WM during maturation [33]. Oligodendrocytes maturate from OPCs through newly formed oligodendrocyte (nfOLG), myelin-forming oligodendrocyte (mfOLG), to mature oligodendrocyte (mtOLG). Studies with AD animal models and AD patients depicted damage in oligodendrocyte lineage cells during disease progress [34, 35]. The primary role of oligodendrocytes is myelination, but oligodendrocytes also support and regulate neurons [36]. Moreover, OPCs are oligodendrocyte lineage cell that directly contacts neurons by making synapses [37]. This functional connectivity between oligodendrocyte and neurons help understand the pathophysiology of AD.

The neurons receive and process the information from other neurons and transmit the signal to other cells in CNS [38]. The neurons in AD show characteristic synaptic losses. The key features of the neurodegenerative process in AD are early synaptic damage with retrograde degeneration of axons [39, 40]. The cognitive impairment in AD patients was found to be closely associated with loss of synapses in the neocortex and limbic system [41, 42]. In addition, dysfunction in

neurons could alter the other cells including oligodendrocytes, thus ultimately affecting behavior [43].

Astrocytes function in neurodevelopment, synaptic modulation, BBB formation, neurovascular coupling, energy metabolism, and response to neuroinflammation. Amyloid beta deposits in AD activate the astrocytes, leading to either beneficial effects by degrading amyloid beta or adverse effects by resulting in dysfunctions between astrocytes and neurons [44]. Astrogliosis was observed in the brains of AD animal models and AD patients in the late stage of the disease [45, 46]. In early studies, astrocytes were binary divided into either 'A1' neurotoxic state or 'A2' neuroprotective state [47]. However, multidimensional studies unraveled that transcriptome of astrocytes were not clearly comply with A1-A2 states. Based on the area where astrocytes were found, astrocytes can be also categorized into protoplasmic and fibrous, or grey matter (GM)-associated and WM-associated astrocytes [48]. Additionally, 'reactive astrocytes' were defined as astrocytes that undergo changes in response to pathological stimuli [49]. The role of each astrocyte subtype under injury or inflammation is currently not clear.

Microglia, as the innate immune cells of the brain, contribute both to injury and repair. Microglia perform neurogenesis, synaptic pruning, and protective role [50], but persistent activation results in

neuroinflammation by ineffective clearance of amyloid beta [51]. A recent study described the microglia subtype, disease-associated microglia (DAM), enrolled in the clearance of amyloid beta, and therefore restrict neurodegeneration in AD [52].

### 1.4 Spatial transcriptomic analysis for the brain

Many discoveries in histopathology of diseases were supported by methods including in situ hybridization by mapping genetic information within tissues. However, these methods provide only limited genetic information. The recent advances in technology enabled to query the whole transcriptome with intact spatial information. This spatially resolved transcriptomics leads to a comprehensive understanding of spatially complexed tissues such as the brain.

#### 1.4.1 Integrative methods for spatial analysis of brain cells

Single-cell RNA sequencing identifies cell population in the tissue while the single-cell isolation step destroys their spatial information. Such spatial information is crucial for understanding the cellular process during the disease process. Spatially resolved transcriptomics offers spatial profiling of quantitative gene expression in tissues [53, 54]. To obtain a comprehensive cellular map and understand their regulatory

logic in the brain, recent approaches focused on the integration of the spatial transcriptome and the single-cell data. These methods define cell type signatures based on gene expression profiles from single-cell data and transfer them into spatial transcriptomic data to predict the distribution of each cell type [55, 56]. Because each spatial spot corresponds to several cell types, comprehensive mapping and analysis of cell types are demanding. Nevertheless, this spatial transcriptomics has great potential to provide detailed cellular maps of diverse tissues.

### 1.5 Final goal of study

To comprehensively understand the mechanism of CNS-targeted drugs, region-specific changes based on the cellular diversity of the brain should be considered. However, there is a lack of research on the central effect of FTY720 on anatomical areas of the brain. This study aims to investigate the pharmacological effect of FTY720 on brain cells according to the anatomical area. These results are expected to provide insights into the cell type-specific and area-specific pathophysiology of AD.

# 2. Methods

## 2.1 Mice data

7-month-old male 5xFAD mice (TG, C57BL/6-SJL background), bearing five FAD mutations in human APP and PS1, were used for spatial transcriptomic data. Non-transgenic littermates were used as wild-type (WT) controls. The study comprised 4 groups of mice: TG treated with FTY720, WT treated with FTY720, untreated TG, and untreated WT (n = 6 for each group). The experimental scheme with the number of animals used was summarized (**Figure 1**). All experimental protocols were approved by the Institutional Animal Care and Use Committee at Seoul National University.

### 2.1.1 Drug protocol

Recent studies of 5xFAD with FTY720 at 0.03-1 mg/kg/day reported decreased accumulation of amyloid beta, decreased activation of glia, and increased neurogenesis [24, 25]. Since a dose of 0.3 mg/kg/day was safe and effective, we added FTY720 into the drinking water at 0.3 mg/kg/day. Mice were treated for 7 weeks since steady-state brain concentration of daily oral administered FTY720 was estimated to be reached after 23 days [57]. Water was changed and monitored

consumption weekly. General condition was checked, and 2 TG with/or without FTY720 showed significant side effects causing death.

### 2.1.2 Behavioral experiments

Y-maze test was performed to evaluate short-term working memory. The mouse was placed at the center of the Y-maze and allowed to move into three arms. The degree of memory impairment was checked by percentage alternation in which the number of entries into three arms was divided by the maximum possible number of entries.

### 2.1.3 Sample preparation

At 8.5 months of age, mice were euthanized by $CO_2$, and brains were collected. For cryosection histology, brains were placed into cryomold with Optimal Cutting Temperature (OCT) media. The tissue embedded in OCT was flash-frozen in a liquid nitrogen-cooled isopentane and stored at -80 °C until sectioning.

### 2.1.4 Immunofluorescence imaging

Paraffin-embedded tissues were sagittally sectioned at 4 μm thickness. Brain sections were deparaffinized with xylenes and rehydrated using a gradient of ethanol. Antigen retrieval was performed by boiling citrate

buffer for 10 min. Tissue sections were blocked with a blocking buffer containing TBS with 0.5% BSA for 1 h. Overnight incubation was performed with mouse β-Amyloid (6E10) (1:100; BioLegend) primary antibody in blocking buffer at 4 °C. The next day, slides were washed with TBS and then incubated with Alexa Fluor secondary antibody (Thermo Fisher Scientific). Finally, the slides were washed and stained with DAPI (1:100; Invitrogen), after which they were mounted with a mounting medium. The slides were imaged using a confocal laser scanning microscope Leica TCS SP8 (Leica, Germany), and the quantitation of β-Amyloid was performed using Metamorph v7.8.10 (Molecular Devices, USA).

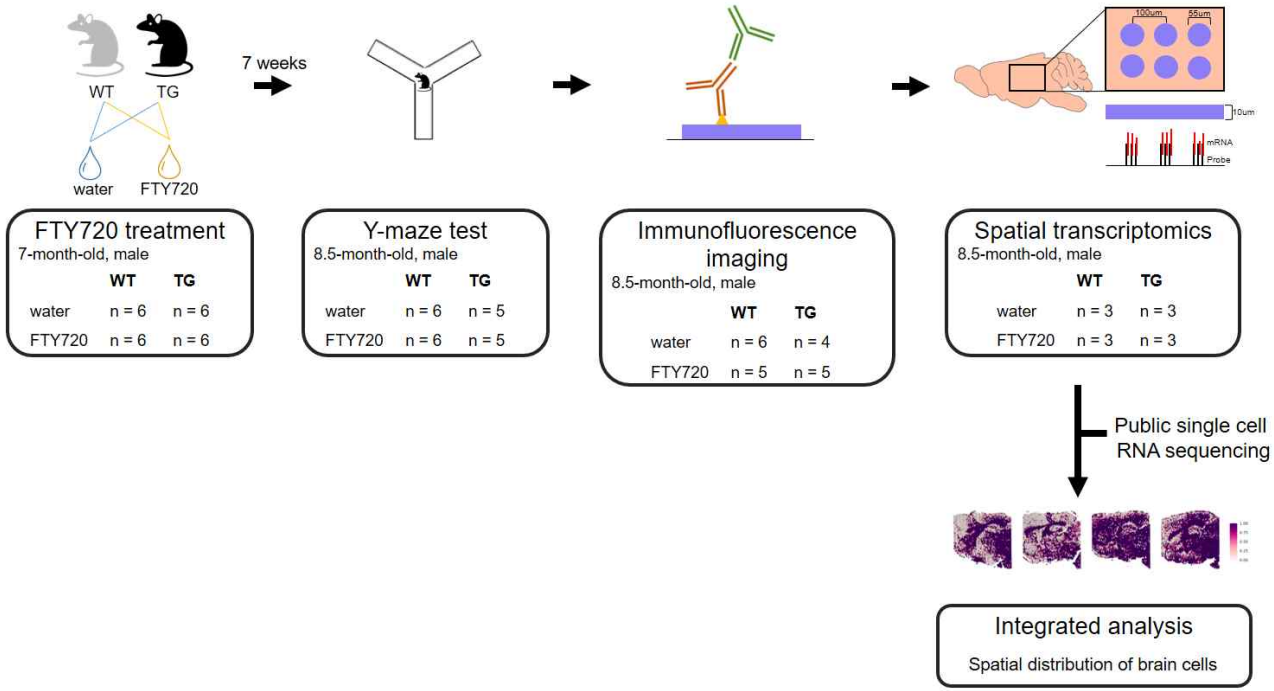


**Figure 1. Schematic diagram of experimental design.** FTY720 at dose of 0.3mg/kg/day was orally administered to 7-month-old male WT and TG for 7 weeks. Y-maze test was performed to evaluate memory deficit, and the pathological change was confirmed using immunofluorescence imaging. The spatial pattern of brain cells was analyzed with adoption of public single-cell RNA sequencing data. WT: C57BL/6J, TG: 5xFAD.

### 2.1.5 Generation of spatial transcriptomic data

10 μm sagittal cryosections were cut and mounted directly on the 10x Visium Spatial Gene Expression Slide (n = 3 for each other group). Tissue sections were methanol-fixed and stained for hematoxylin and eosin (H&E). Bright-field images of stained sections were obtained before the permeabilization. After the permeabilization, released mRNAs are processed for cDNA library preparation. cDNA libraries were sequenced on Illumina NovaSeq 6000 (Illumina, USA).

Raw FASTQ data from sequencing and H&E images were processed using the 10x SpaceRanger v1.1 pipelines. Samples from the Illumina sequencing were converted to FASTQ files using mkfastq pipeline. In addition, a count pipeline was used to align FASTQ files with bright-field images, detect unique molecular identifier (UMI), and map sequencing reads to mm10 reference genome (mm10-2020-A) using STAR v2.5.1b aligner.

### 2.1.6 Clustering of spatial transcriptomic data

The spots with gene expression data were analyzed using Seurat package v4.0.6 [56]. The gene counts were normalized using 'LogNormalize' method. The top 2000 highly variable genes were identified using 'vst' method. During the data scaling, the number of RNA counts and

percentage of mitochondrial genes for each spot was regressed out. Four spatial transcriptomic datasets were merged and rescaled. The top highly variable genes were used for principal component analysis. Dimension reduction was performed with UMAP based on the top 30 principal components. Clustering based on the Louvain community detection algorithm was processed with a resolution of 0.2. For the visualization of spot clusters, a uniform manifold approximation and projection (UMAP) plot was generated. Markers for each cluster were identified using FindAllMarkers function. Each sample was segmented into nine anatomical regions (septum, striatum, white matter, cortex, hippocampus, thalamus, hypothalamus, midbrain, and ventricle) using Allen Brain Reference Atlas [58]. Enrichment analyses including Gene Ontology (GO) and Kyoto Encyclopedia of Genes and Genomes (KEGG) pathway analyses for area-specific markers were performed with clusterProfiler [59].

### 2.1.7 Analysis of sphingolipid pathway

Since FTY720 targets S1PRs, expression patterns of S1PRs subtype were evaluated. In addition, a gene set related to downstream signaling of S1PRs was selected from Mouse Genome Informatics (MGI): *Akt1*, *Ezr*, *Pik3cb*, *Pik3cg*, *Rac1*, and *Spns2*. The signature score for S1PRs

downstream signaling pathway was calculated with the AddModuleScore function. The genes constituting each score were visualized by SpatialFeaturePlot function for identifying spatial distribution patterns.

### 2.1.8 Weighted gene co-expression network analysis (WGCNA)

The WGCNA package in R was implemented and the network was constructed using genes that expressed at transcripts per million reads the value of 1 or higher in all spots. Average linkage hierarchical clustering was applied to group genes into modules.

## 2.2 Public data

Publicly available single-cell datasets of the brain were selected by a thorough literature search. To reduce the discrepancy between spatial data and publicly available single-cell datasets, mouse model, location of the sample, and analyzed cell type of single-cell datasets were considered. The characteristics of the data are summarized in **Table 1**.

### 2.2.1 Clustering of single-cell data

The count of single-cell data was log-normalized in the same way as

spatial transcriptomic data. After the selection of the top 2000 highly variable genes, the total count in each spot was regressed out during the data scaling. Principal component analysis was performed followed by single-cell clustering. The resolution for clustering was determined according to the datasets. UMAP plot was drawn to visualize cell clusters. Additionally, subsets for cell subtypes were extracted and processed in the following order: rescaling, principal component analysis, and clustering. Each cluster was named after annotation information or cell markers that have been previously described in the literature.

### 2.2.2 Single-cell data: whole brain cells of mice

Single-cell RNA sequencing data from the forebrain and midbrain of 2-month to 3-month-old and 21-month to 23-month-old C57BL/6J mice were adopted [60] and integrated with spatial transcriptomic data. The count matrix was composed of 37069 cells and 16499 genes. Total of 25 cell clusters were made and the name of each cell type was named after provided information which was based on the cell marker genes. For the subtype analysis of oligodendrocyte lineage cells and mature neurons, single-cell data was selected using a subset function. Oligodendrocyte lineage cells (14699 cells) were composed of oligodendrocyte precursor cell (OPC) and oligodendrocytes (OLG), and oligodendrocytes were

further classified as nfOLG, mfOLG, and mtOLG. Neuronal lineage cells (5773 cells) were subdivided into neuronal-restricted precursor (NRP), Immature neuron (ImmN), neuroendocrine cell (NendC), and neurotransmitter-expressing populations: GABAergic, glutamatergic, dopaminergic, and cholinergic neurons.

| Model mouse | Sex | Age | Area | Cell types | References |
|---|---|---|---|---|---|
| C57BL/6J | Male | 2-3 mon<br>21-23 mon | Forebrain,<br>Midbrain | Whole brain cells | Ximerakis et al., 2019 |
| CD-1 or C57BL/6J<br>TG (CD-1 or C57BL/6J background) | Male/ Female | P21-P30<br>P60 | Somatosensory cortex, Striatum, Dentate Gyrus, Hippocampus, Corpus callosum, Amygdala, Hypothalamus,<br>Zona incerta,<br>Substantia nigra, Dorsal horn | Oligodendrocyte lineage cells enriched | Marques et al., 2016 |
| TG (C57BL/6J background) | Male/ Female | P53-59<br>P50-52<br>P60-121 | Cortex,<br>Hippocampus | Neuron enriched | Yao et al., 2021 |
| C57BL/6J | Male/ Female | P56 | Cortex,<br>Hippocampus | Astrocyte enriched | Batiuk et al., 2020 |
| C57BL/6J<br>TG (5xFAD) | Male/ Female | 1-9 mon | Whole brain | CD45+ enriched | Keren-Shaul et al., 2017 |

**Table 1. Characteristics of single-cell datasets**

### 2.2.3 Single-cell data: oligodendrocytes of mice

Single-cell datasets were obtained from CD-1 or C57BL/6J based WT and TG between post-natal days 21 and 60 [61]. Distinctive 10 regions of the brain were included. To enrich oligodendrocyte lineage cells, cells with oligodendrocyte lineage labels were FACS sorted. The transcriptome comprises 5069 cells and 23556 genes. Cell types were annotated regarding literature-based cell markers.

### 2.2.4 Single-cell data: neurons of mice

The cortex and hippocampus of transgenic mice with C57BL/6J background were extracted for single-cell sequencing [62]. Neuron-enriched single-cell sequencing was performed with the help of retrograde and retro-orbital labeling. As a result, a count matrix with 72746 cells and 45768 genes was made. A total of 4 classes and 43 cell clusters were created and named after the provided annotation.

### 2.2.5 Single-cell data: astrocytes of mice

The cortex and hippocampus of C57BL/6J mice aged to post-natal day 56 were obtained for single-cell sequencing [63]. Astrocytes were FACS isolated and underwent sequencing, which resulted in a count matrix for 1811 cells and 49660 genes. Five astrocyte clusters were labeled by the

paper.

### 2.2.6 Single-cell data: CD45+ cells of mice

The whole brain including meninges and choroid plexus of 1-month to 9-month-old C57BL/6 and 5XFAD mice were obtained and CD45+ cells were sorted [52]. The count matrix with 25944 cells and 33924 genes was integrated with spatial data. The cell types including homeostatic microglia and DAM were assigned based on the marker genes from the literature.

## 2.3 Integrative analysis of spatial data and single-cell data

### 2.3.1 NS-Forest method

The optimal combinations of markers from single-cell data were selected using Necessary and Sufficient Forest (NS-Forest) v2.0 [64]. Based on the random forest machine learning and binary expression scores, NS-Forest provides minimum sets of marker genes for specific cell types. Selected marker genes were used for scoring each cell type. The cell type scores were calculated using the AddModuleScore function, which finds the average expression level, compared to the mean expression levels across the dataset. The cell type scores were mapped into spatial data by SpatialPlot function.

### 2.3.2 CellDART method

The CellDART, an analysis method that joints single-cell data and spatial data by the adversarial domain adaptation method, was used to predict the fraction of each cell type in a spatial spot [65]. Randomly sampled cells from single-cell data generate a pseudospot with known cell fraction. The model that predicts the cell fraction of psuedospot from gene expression was adopted to the spatial trancriptomics domain. The calculated cell fractions were spatially mapped using SpatialPlot function.

### 2.3.3 DestVI method

The DestVI, deconvolution of spatial transcriptomics profiles using variational inference, is a recently developed method to estimate gene expression for every cell type in every spot of the spatial transcriptome [66]. Although integration of single-cell data and spatial data could calculate the proportion of each cell type within each spot, there has been no possible way to extract cell type-specific transcription at every spot. Single-cell data and spatial data are used to make two latent variable models, and DestVI outputs the estimated proportion of cell type in each spot and projects the expression of each spot onto latent spaces composed of each cell type.

### 2.4 Statistical analysis

All data were statistically analyzed with R. The comparison of features of brain cells between different mice was conducted by the Kruskal Wallis test. The correlation between the alternation and the features of spatial transcriptomics was estimated by the Spearman correlation.

# 3. Results

## 3.1 Behavioral change in Alzheimer's disease model mice

In the Y-maze test, changes in working memory according to the FTY720 treatment were confirmed. No statistically significant change in behavior was found between WT control and TG control. Both WT and TG mice showed significant enhancement in alternation when FTY720 was administered (**Figure 2**). Three representative mice in each group were selected for spatial transcriptomics.

## 3.2 Immunofluorescence imaging in Alzheimer's disease model mice

Immunofluorescence of Aβ on the sagittal sections of the brain was measured. In addition, regional images showing immunofluorescence of Aβ were captured. Among regions including septum and striatum, WM, cortex, and hippocampus, FTY720 showed no significant change in Aβ deposits in every included area (**Figure 3**).

## 3.3 Spatial pattern in Alzheimer's disease model mice

### 3.3.1 Spatial spot-based analysis

Sagittal sections of the whole brain that contain diverse cell types across anatomical regions in WT and TG with or without FTY720 were

examined (**Figure 4**). Based on the transcriptomics profiles of highly variable genes, the tissue regions represented as spatial spots were divided into 19 clusters and visualized using UMAP. These clusters were aligned with anatomical brain regions.

The average expression of the top 5 marker genes in each anatomical area was visualized with a heatmap (**Figure 5**). To characterize the biological profiles associated with a specific area, pathway analyses using GO and KEGG were performed. Genes of WM were associated with gliogenesis, ensheathment of neurons, and myelination.

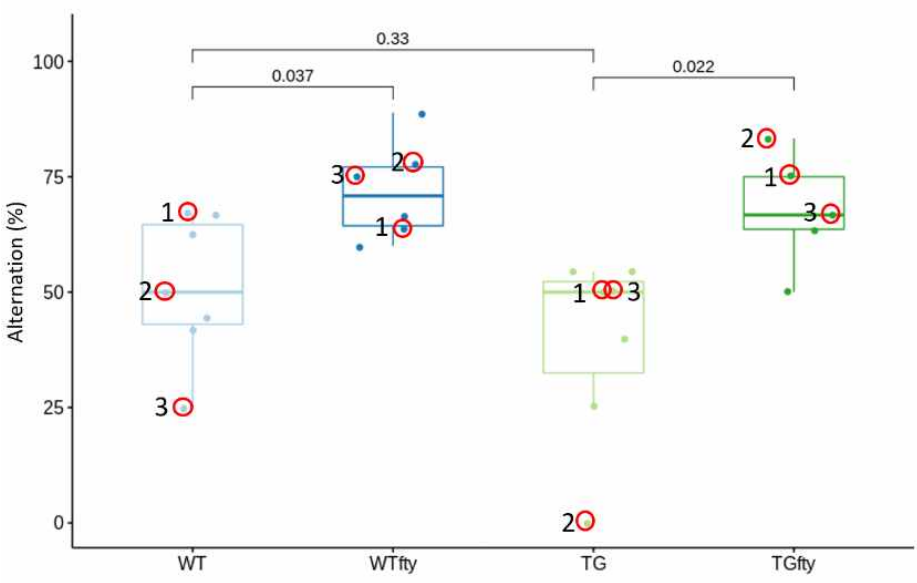


**Figure 2. Alternation change in Y-maze test.** FTY720 treatment induced significant improvement of behavior compared to the untreated control. The selected mice for spatial transcriptomic analysis were red-circled. WT: C57BL/6J, WTfty: C57BL/6J with FTY720, TG: 5xFAD, TGfty: 5xFAD with FTY720.

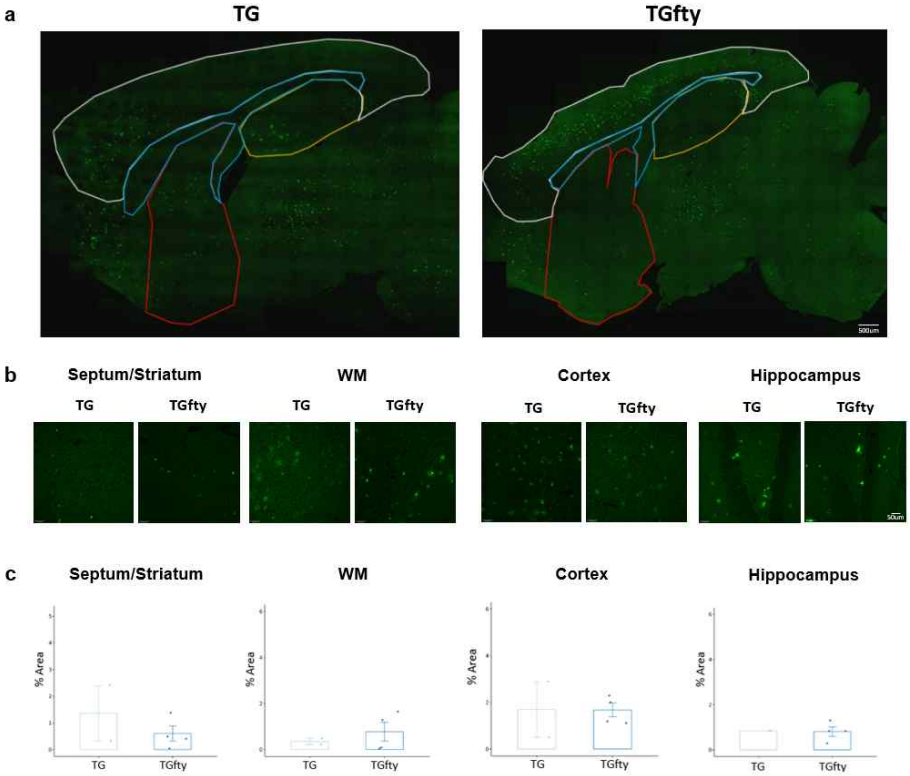


**Figure 3. Pathological change in Alzheimer's disease model mice by FTY720.** (a) Whole brain images of Aβ immunostaining in TG and TGfty. Red area for septum/striatum, skyblue area for WM, white area for cortex, yellow area for hippocampus. (b) Regional images of Aβ immunostaining in TG and TGfty. (c) Bar plots of average immunofluorescence in each area. The deposition of Aβ showed no significant change by FTY720. TG: 5xFAD, TGfty: 5xFAD with FTY720, WM: white matter.

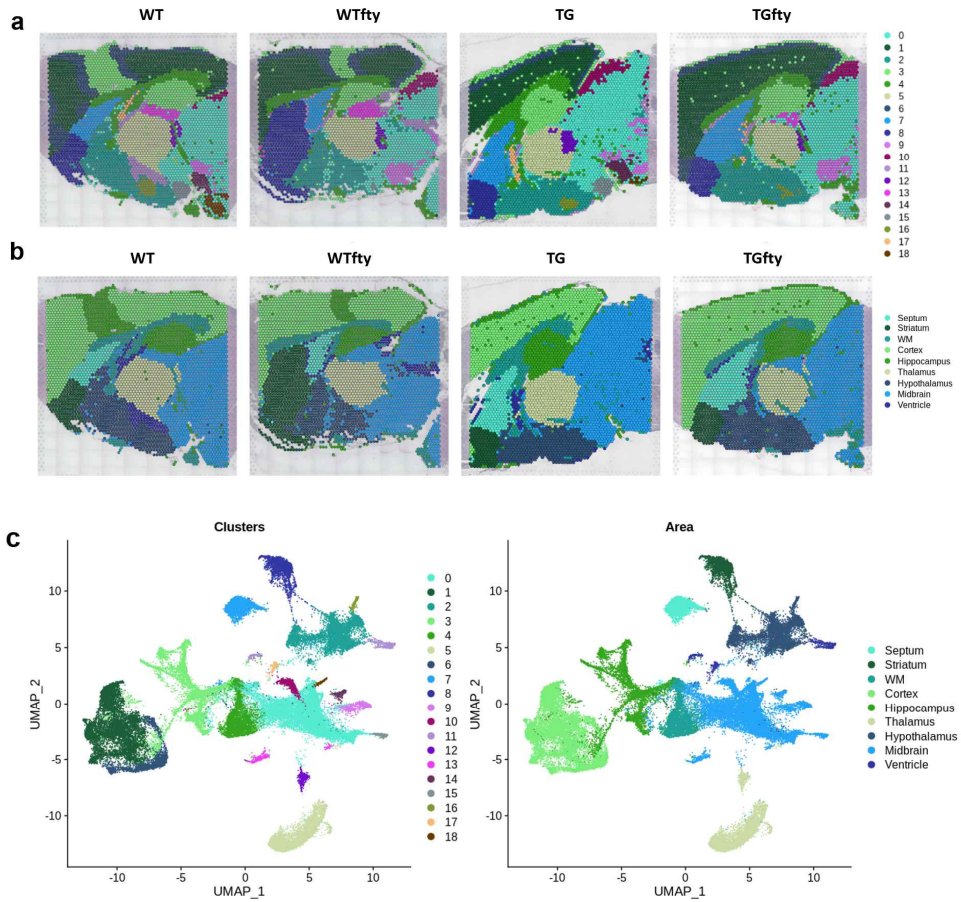
a
WT
WTfty
TG
TGfty
0
1
2
3
4
5
6
7
8
9
10
11
12
13
14
15
16
17
18
b
WT
WTfty
TG
TGfty
Septum
Striatum
WM
Cortex
Hippocampus
Thalamus
Hypothalamus
Midbrain
Ventricle
c
Clusters
Area
UMAP_2
UMAP_1
10
5
0
-5
-10
Septum
Striatum
WM
Cortex
Hippocampus
Thalamus
Hypothalamus
Midbrain
Ventricle

**Figure 4. Spot clustering of Visium spatial transcriptomic data.** (a) Clustering of spots for WT and TG sagittal sections, labeled with cluster number and (b) with anatomical location. (c) A 19 clusters were classified either into cluster or anatomical area and visualized on UMAP. WT: C57BL/6J, WTfty: C57BL/6J with FTY720, TG: 5xFAD, TGfty: 5xFAD with FTY720, WM: white matter.

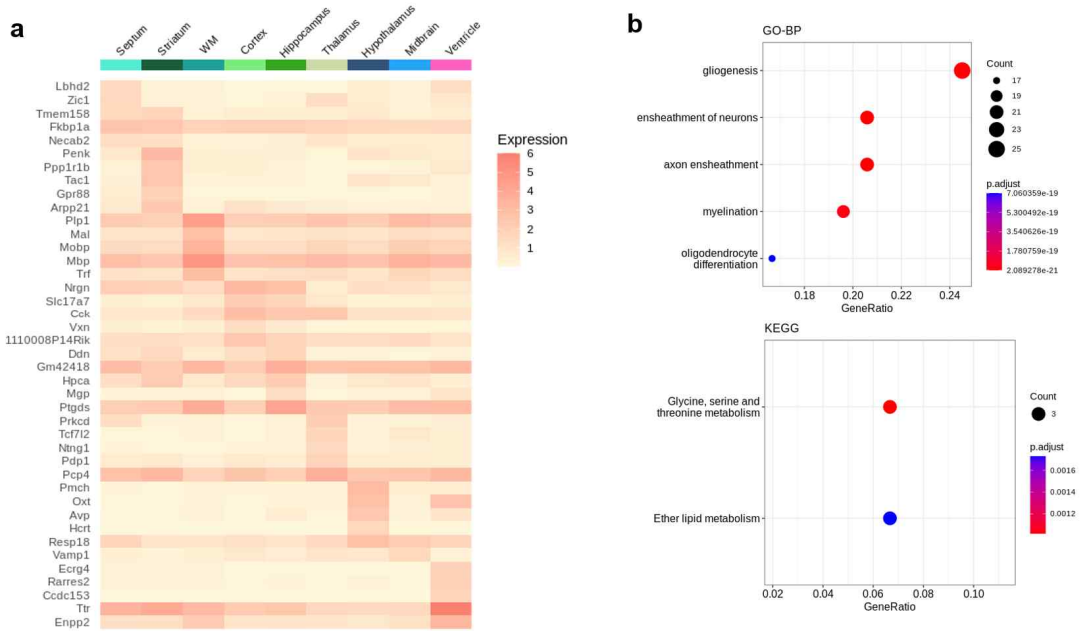


**Figure 5. Top 5 marker genes in each area.** (a) A heatmap of average expression of top 5 marker genes in each anatomical area. (b) GO and KEGG pathway analyses for marker genes of the WM. GO-BP: Gene Ontology-Biological Pathway, KEGG: Kyoto Encyclopedia of Genes and Genomes.

### 3.3.2 Sphingolipid features

As one of the ways to assess whether FTY720 directly induces expression of the brain transcriptome, expression and spatial pattern of S1PRs were investigated (**Figure 6**). Expression levels of S1PRs in each region were averaged and presented as a heatmap. *S1pr1* was the most abundantly expressed subtype among S1PRs. The expression of *S1pr5* was dominant in the WM. TG showed overall downregulation of S1PRs compared to WT. However, FTY720 restored the downregulation of *S1pr1* and *S1pr5* in the WM of TG. S1PRs and features related to the downstream pathway of S1PRs were spatially represented. *S1pr1* was located in the WM, striatum, cortex, and hypothalamus of WT. This spatial pattern of *S1pr1* was localized except for the WM of TG but recovered after FTY720 treatment. *S1pr5* was mainly restricted to the WM, where only TG showed a marked decrease. The features of S1PRs downstream pathway were located in the WM, cortex, and striatum. Genes related to downstream signaling of S1PRs were downregulated in WM of TG but reversed by FTY720.

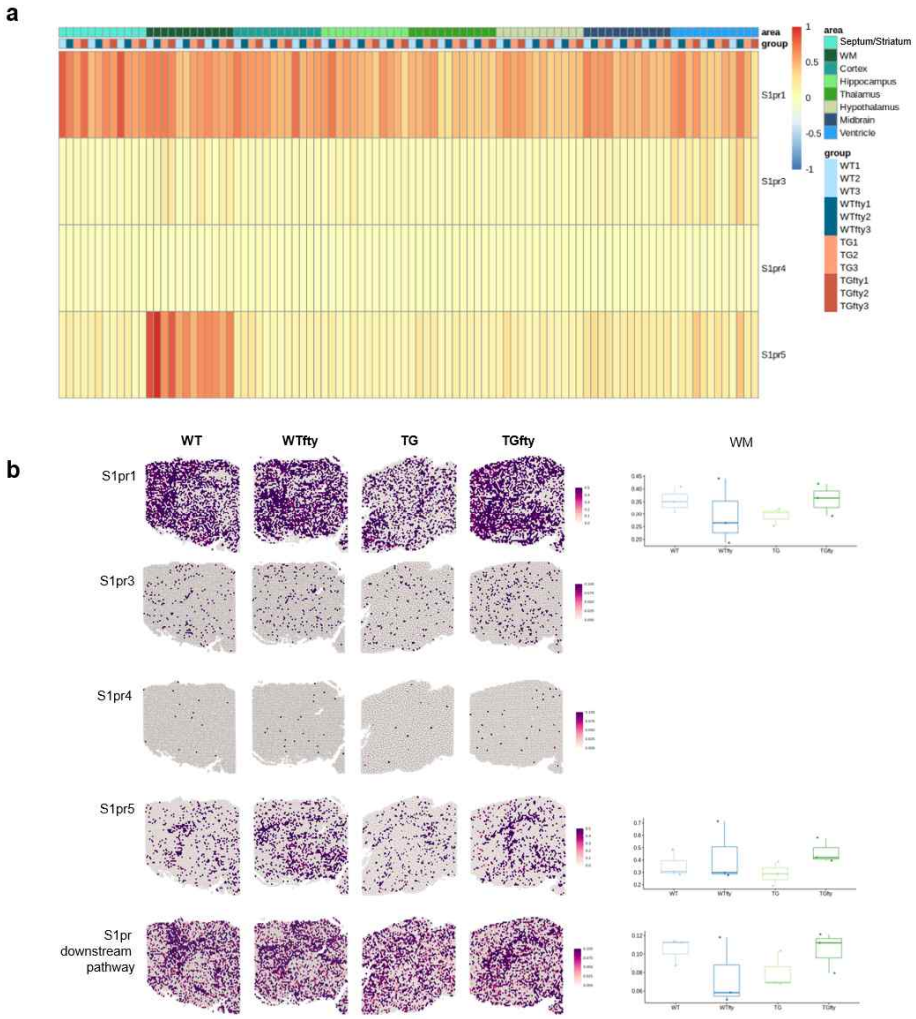


**Figure 6. Spatial map of sphingolipid features.** (a) A heatmap of average expression of S1PRs in anatomical area. (b) Spatial maps of S1PRs and feature of S1PRs downstream pathway. Expression of *S1pr1*, *S1pr5*, and genes related to S1PR downstream pathway were downregulated in the WM of TG, but restored by FTY720. Box and Whisker plots of average expression of each feature in WM. WT: C57BL/6J, WTfty: C57BL/6J with FTY72, TG: 5xFAD, TGfty: 5xFAD with FTY720, S1PRs: sphingosine-1- phosphate receptors.

### 3.3.3 Module-based analysis

A total of 11 modules including pink, red, and blue were obtained (**Figure 7**). When the modules were mapped to the brain sagittal sections, each module showed a distinctive spatial pattern. The pink module was localized in the 'T' shaped WM. The red module was distributed in the 'cone' shaped striatum. The blue module was presented in the cortex, hippocampus, and striatum. To characterize the biological profiles of pink, red, and blue modules, pathway analysis using GO was performed. Pathways including gliogenesis and glial cell differentiation characterized the pink module. Red and blue modules were related to the common pathway of learning.

Module scores were also evaluated versus cell fractions that had been calculated by CellDART method (**Figure 8**). The pink module had a strong positive correlation with oligodendrocyte and a rather negative correlation with OPC and mature neuron. Red and blue modules showed a positive correlation with mature neuron and OPC, whereas a negative correlation with oligodendrocyte.

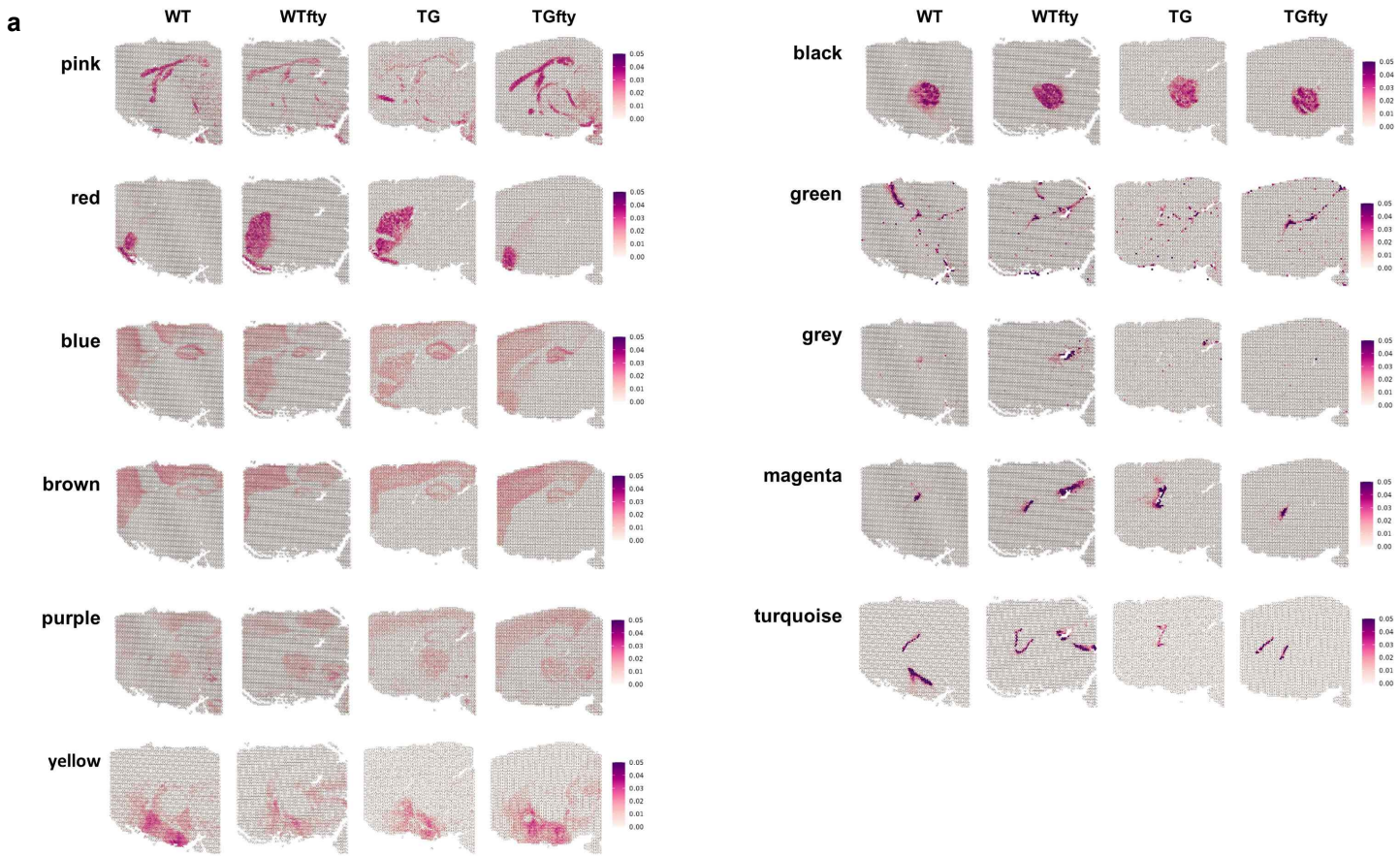
a
WT
WTfty
TG
TGfty
pink
red
blue
brown
purple
yellow
black
green
grey
magenta
turquoise
0.05
0.04
0.03
0.02
0.01
0.00

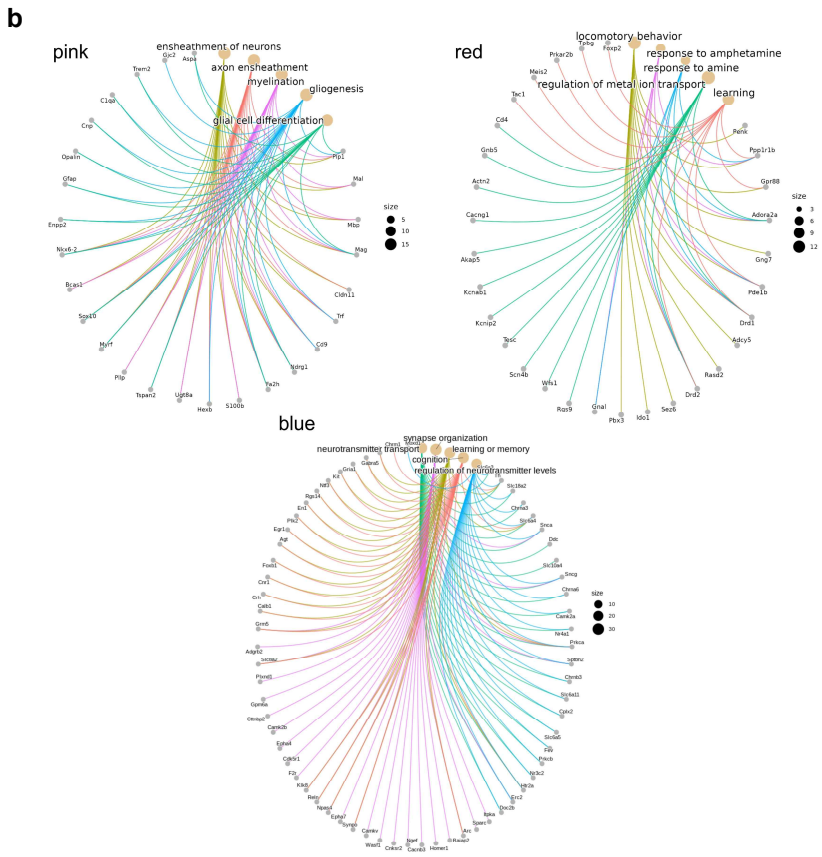


**Figure 7. Spatial characteristics of WGCNA modules.** (a) A total of 11 modules from WGCNA were mapped in the Visium data. Each module in which consisted with closely connected genes showed distinctive pattern. Pink and red modules were mainly localized in the WM and the striatum, respectively. The blue module was located in the cortex, hippocampus, and striatum. (b) GO results of pink, red, and blue modules were presented. Pink module was related to gliogenesis and myelination, while red and blue modules shared functional pathways related to learning. WT: C57BL/6J, WTfty: C57BL/6J with FTY720, TG: 5xFAD, TGfty: 5xFAD with FTY720, WGCNA: Weighted gene co-expression network analysis, GO: Gene Ontology.

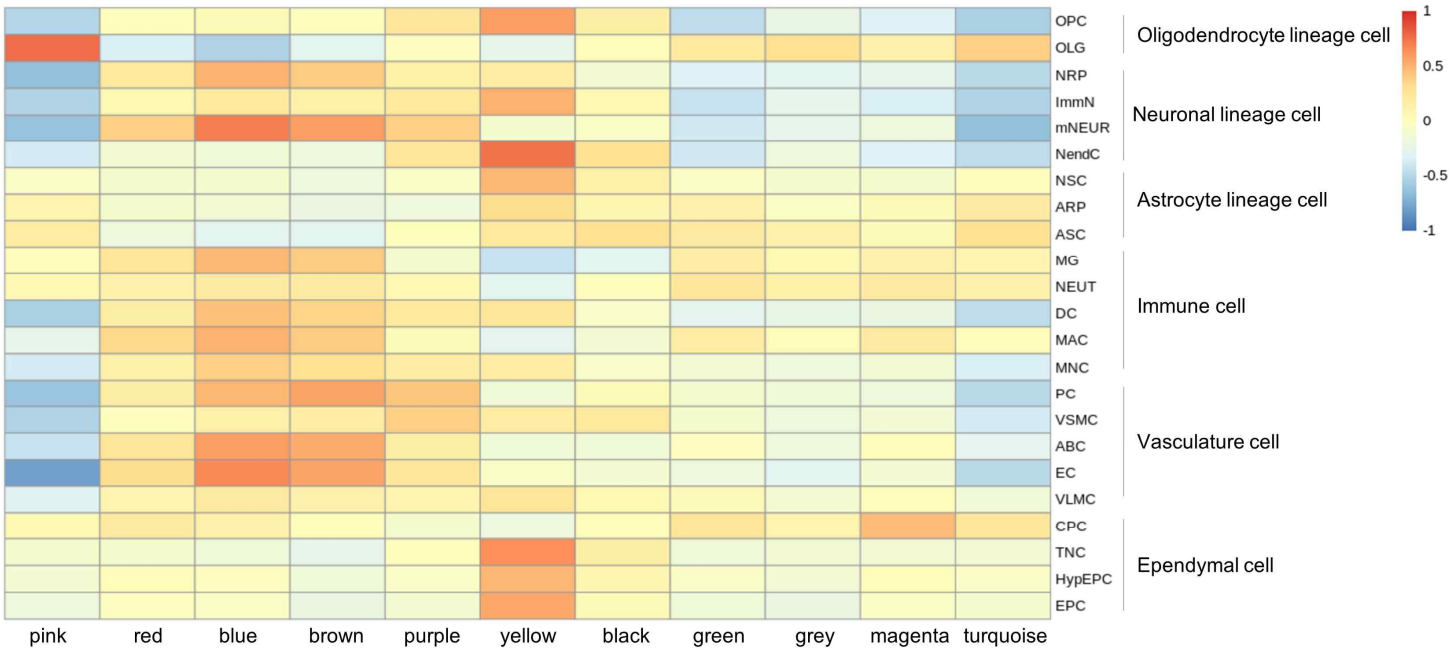


**Figure 8. Correlation between CellDART-based cell fraction and WGCNA modules.** A heatmap of Spearman's correlation coefficient between WGCNA module score and cell fraction calculated with CellDART. Positive correlations were found between pink module and oligodendrocyte, red and blue modules with mature neuron and OPC. OPC: oligodendrocyte precursor cell, OLG: oligodendrocyte, NRP: neuronal-restricted precursor, ImmN: immature neuron, mNEUR: mature neuron, NendC: neuroendocrine cell, NSC: neural stem cell, ARP: astrocyte-restricted precursor, ASC: astrocyte, MG: microglia, NEUT: neutrophil, DC: dendritic cell, MAC: macrophage, MNC: monocyte, PC: pericyte, VSMC: vascular smooth muscle cell, ABC: arachnoid barrier cell, EC: endothelial cell, VLMC: vascular and leptomeningeal cell, CPC: choroid plexus epithelial cell, TNC: tanycyte, HypEPC: hypendymal cell, EPC: ependymocyte.

### 3.4 Spatial distribution of major brain cells

Major brain cells including oligodendrocyte, neuron, astrocyte, and microglia were spatially mapped in sagittal sections of WT and TG mice (**Figure 9**). Cell-specific marker genes based on NS-Forest were used for the calculation of the feature score of each cell type (**Table 2**). The oligodendrocytes of WT were restricted to the WM, thalamus, striatum, and midbrain. Notably, a spreading pattern from WM to the adjacent deeper layer of cortex and septum or striatum of oligodendrocyte was found in TG. However, this pattern was restored when FTY720 was treated to TG. The spatial distribution of neuron was localized in the cortex, striatum, and thalamus, which consistent among groups. Astrocyte and microglia showed spatial spread to the cortex, striatum, thalamus, and midbrain in TG compared to WT, however, no significant difference was observed between TG with FTY720 and TG control. Spatial mapping of brain cells was also confirmed using the CellDART. Fractions of each cell type were estimated by the CellDART applied on a spatial map. The patterns of each cell type based on the CellDART method were similar to the spatial distribution of each cell type by the NS-Forest method.

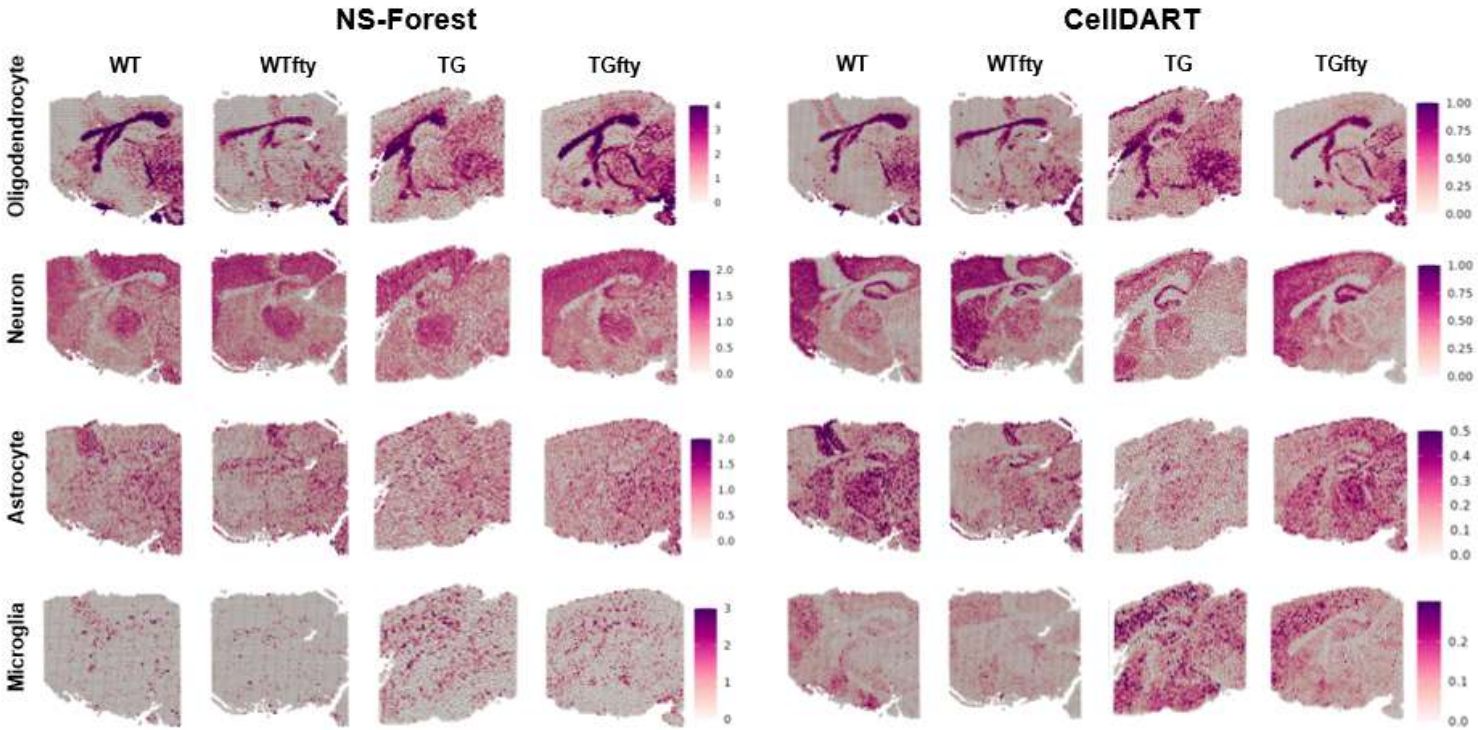


**Figure 9. Spatial map of major cell types.** The major brain cells including oligodendrocyte, neuron, astrocyte, and microglia were spatially distributed. Two methods, NS-Forest and CellDART were used for cell type-specific mapping. Oligodendrocyte showed spreading pattern from the WM to adjacent anatomical areas in TG, whereas FTY720 restored it similar to the distribution in WT. WT: C57BL/6J, WTfty: C57BL/6J with FTY720, TG: 5xFAD, TGfty: 5xFAD with FTY720, NS-Forest: Necessary and Sufficient Forest.

| Cell type | Marker genes |
|---|---|
| **Oligodendrocyte** | *Mobp*, *Cldn11*, *Cnp*, *Mal*, *Plp1*, *Stmn4*, *Car2*, *Gatm*, *Cryab*, *Fth1* |
| **Neuron** | *Gad1*, *Synpr*, *Camk2b*, *Ndrg4*, *Syt1*, *Snap25*, *Snhg11*, *Celf4*, *Atp1b1*, *Meg3* |
| **Astrocyte** | *Cldn10*, *Ntsr2*, *Gjb6*, *Gm3764*, *Gja1*, *Plpp3*, *Aldoc*, *Mt3*, *Mt1*, *Apoe* |
| **Microglia** | *Siglech*, *Tmem11*, *P2ry12*, *Cx3cr1*, *Hexb*, *Trem2*, *Selplg*, *C1qb*, *Ly86*, *Ctss* |

**Table 2. NS-Forest-based marker genes of major brain cell types**

### 3.4.1 Spatial characteristics of oligodendrocyte lineage cells

The subtypes of oligodendrocyte lineage cells were classified by literature-based markers (**Figure 10**). A total of 25 cell types from aging mouse single-cell RNA sequencing data were visualized on UMAP. Subtypes of oligodendrocyte lineage cells were identified based on the expression of the marker genes: *Pdgfra* for OPC; *Tmem2* for nfOLG; *Ctps* for mfOLG, and *Apod* for mtOLG. The spatial distributions of fractions of oligodendrocyte lineage cells based on CellDART were presented. In TG, nfOLG and mfOLG had increased spatial distribution in the thalamus and cortex, while no significant change was seen in OPC and mtOLG. Moreover, the spatial distribution of mfOLG in the WM that was decreased in TG was dramatically recovered when the TG was treated with FTY720. The fractions of each oligodendrocyte lineage cell in other areas including the cortex, septum, striatum, hippocampus, and thalamus remained constant despite the FTY720.

Oligodendrocyte-enriched single-cell data was adopted as a reference, and the cell annotation labels from the reference were transferred to whole brain single-cell data **(Supplementary figure 1a)**. Adjusted labels based on the cell annotation method newly classified differentiation-committed oligodendrocyte precursor (COP). The spatial distribution of COP was similar to the pattern of OPC. The spatial maps

of nfOLG, mfOLG, and mtOLG based on adjusted labels were similar to the spatial maps of nfOLG, mfOLG, and mtOLG based on literature-based classification.

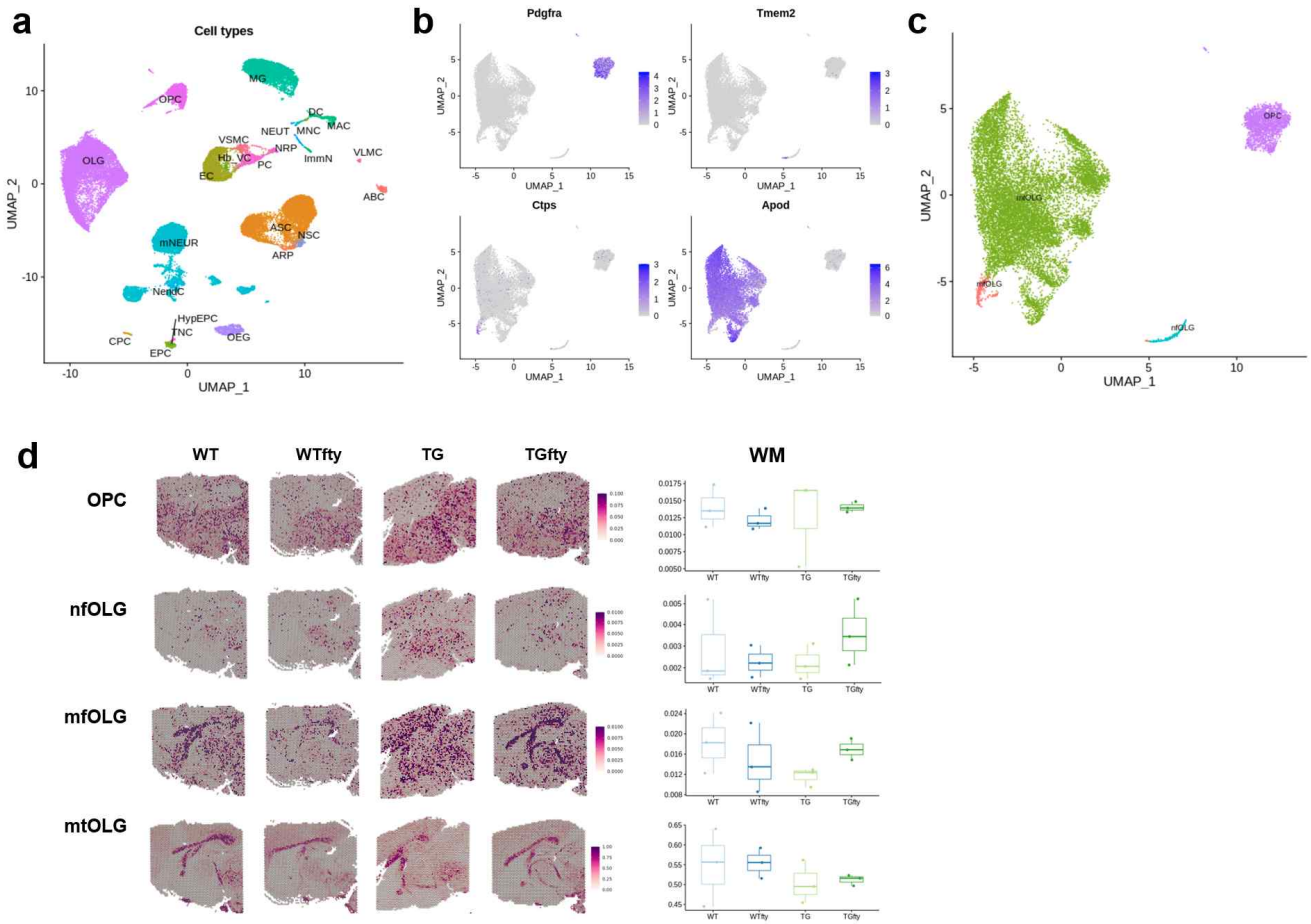
a
Cell types
MG
OPC
DC
MAC
NEUT
MNC
VSMC
NRP
VLMC
OLG
Hb_VC
PC
ImmN
EC
ABC
ASC
NSC
mNEUR
ARP
NeuIC
HypEPC
TNC
OEG
CPC
EPC
UMAP_1
UMAP_2
b
Pdgfra
Tmem2
Ctps
Apod
c
OPC
mfOLG
nfOLG
d
WT
WTfty
TG
TGfty
WM
OPC
nfOLG
mfOLG
mtOLG

**Figure 10. Spatial map of oligodendrocyte lineage cells.** (a) A UMAP of single-cell data of whole brain cells and oligodendrocyte lineage cells were selected (grey circle). (b) Marker genes used for oligodendrocyte lineage cell type labeling. *Pdgfra* for OPC, *Tmem2* for nfOLG, *Ctps* for mfOLG, and *Apod* for mtOLG. (c) UMAP showing single-cell data of whole brain cells. (d) Oligodendrocyte lineage cells were distributed on sagittal sections. The labels of oligodendrocyte lineage cells were obtained from literature-based marker genes. Regional specificity was observed in all oligodendrocyte lineage cells. In TG, FTY720 mediated spatial restriction, which was similar to the pattern shown in WT. Box and Whisker plots of average fractions of oligodendrocyte lineage cells in WM. mfOLG of TG showed increased fraction in WM by FTY720. WT: C57BL/6J, WTfty: C57BL/6J with FTY720, TG: 5xFAD, TGfty: 5xFAD with FTY720, OPC: oligodendrocyte precursor cell, OLG: oligodendrocyte, NRP: neuronal-restricted precursor, ImmN: immature neuron, mNEUR: mature neuron, NendC: neuroendocrine cell, NSC: neural stem cell, ARP: astrocyte-restricted precursor, ASC: astrocyte, MG: microglia, NEUT: neutrophil, DC: dendritic cell, MAC: macrophage, MNC: monocyte, PC: pericyte, VSMC: vascular smooth muscle cell, ABC: arachnoid barrier cell, EC: endothelial cell, VLMC: vascular and leptomeningeal cell, CPC: choroid plexus epithelial cell, TNC: tanycyte, HypEPC: hypendymal cell, EPC: ependymocyte, nfOLG: newly formed oligodendrocyte, mfOLG: myelin-forming oligodendrocyte, mtOLG: mature oligodendrocyte, WM: white matter.

### 3.4.2 Spatial characteristics of neuronal lineage cells

The neuronal lineage cells from the whole brain single-cell were mapped to the sagittal sections (**Figure 11**). Neuronal lineage cells were classified according to the expression of literature-based marker genes: *Cdk1* for NRP and ImmN; *Baiap3* for NendC; *Gad1* for GABAergic; *Slc17a7* for glutamatergic; *Th* for dopaminergic; and *Slc18a3* for cholinergic neurons. The spatial fractions of NRP, ImmN, and cholinergic neurons were markedly small and adjustment of the scale bar was inevitable. Although the fractions of NRP and ImmN were increased in TG, no spatial change was observed when FTY720 was treated in TG. The spatial patterns of NendC, GABAergic, and cholinergic neurons were similar among different groups. The glutamatergic neuron of TG showed an increased fraction in the cortex, but FTY720 decreased its cortical fraction. Dopaminergic neurons showed decreased fraction in the ventral tegmental area (VTA) of TG. FTY720 restored the distribution of the dopaminergic neurons in VTA. Single-cell dataset of the neuron-enriched sample, composed of glutamatergic and GABAergic neurons, was also mapped for Visium data (**Supplementary figure 1b**). The spatial patterns of both neuronal subtypes of neuron-enriched single-cell data were similar to the patterns of glutamatergic and GABAergic neurons of whole brain single-cell [67].

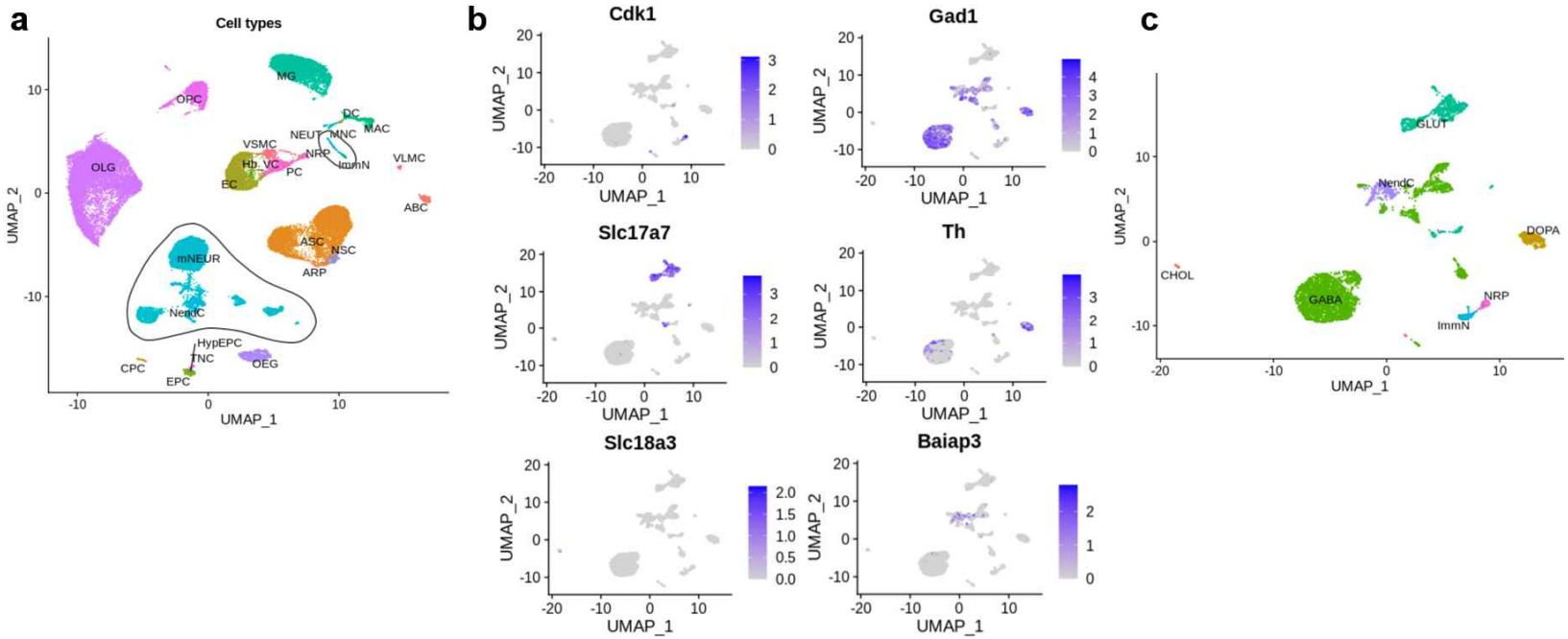
a
Cell types
MG
OPC
DC
MAC
NEUT
MNC
VSMC
Hb_VC
NRP
ImmN
VLMC
OLG
EC
PC
ABC
ASC
NSC
mNEUR
ARP
NendC
HypEPC
TNC
CPC
OEG
EPC
UMAP_2
UMAP_1
b
Cdk1
Gad1
Slc17a7
Th
Slc18a3
Baiap3
c
GLUT
NendC
DOPA
CHOL
GABA
NRP
ImmN

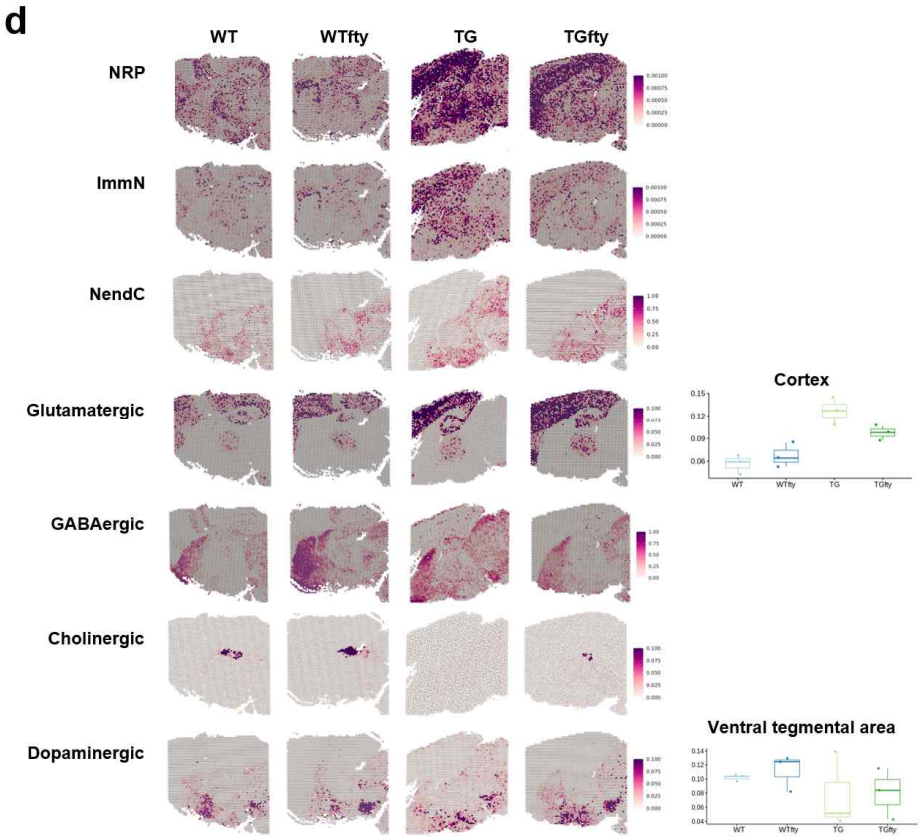


**Figure 11. Spatial map of neuronal lineage cells.** (a) A UMAP of single-cell data of whole brain cells and neuronal lineage cells were selected (grey rings). (b) Marker genes used for neuronal lineage cell type labeling. *Cdk1* for NRP and ImmN, *Gad1* for GABA, *Slc17a7* for GLUT, *Th* for DOPA, *Slc18a3* for CHOL, and *Baiap3* for NendC. (c) UMAP of neuronal lineage cells. (d) Neuronal lineage cells of whole brain single-cell were mapped on sagittal sections. Box and Whisker plots for average fractions of neuronal lineage cells in each representative area. WT: C57BL/6J, WTfty: C57BL/6J with FTY720, TG: 5xFAD, TGfty: 5xFAD with FTY720, OPC: oligodendrocyte precursor cell, OLG: oligodendrocyte, NRP: neuronal-restricted precursor, ImmN: immature neuron, mNEUR: mature neuron, NendC: neuroendocrine cell, NSC: neural stem cell, ARP: astrocyte-restricted precursor, ASC: astrocyte, MG: microglia, NEUT: neutrophil, DC: dendritic cell, MAC: macrophage, MNC: monocyte, PC: pericyte, VSMC: vascular smooth muscle cell, ABC: arachnoid barrier cell, EC: endothelial cell, VLMC: vascular and leptomeningeal cell, CPC: choroid plexus epithelial cell, TNC: tanycyte, HypEPC: hypendymal cell, EPC: ependymocyte, GABA: GABAergic neuron, GLUT: glutamatergic neuron, DOPA: dopaminergic neuron, CHOL: cholinergic neuron.

### 3.4.3. Spatial characteristics of astrocyte subtypes

Two subtypes of astrocyte were defined by literature-based marker genes (**Table 3**) [68] and integrated with Visium data (**Figure 12**). GM-associated astrocytes and WM-associated astrocytes were mainly located in the GM and WM, respectively. In TG, both GM-associated astrocytes and WM-associated astrocytes were increased in the cortex, septum, striatum, and thalamus. Under FTY720, GM-associated astrocytes were decreased in the cortex. WM-associated astrocytes were increased in WM of TG, but no transcriptional change by FTY720 was found. The spatial patterns of GM-associated astrocytes in WM were consistent among groups. An additional astrocyte subtype was evaluated, named reactive astrocyte by using literate suggested marker genes [49]. Reactive astrocytes were increased in the septum, striatum, cortex, WM, and thalamus in TG, but there was no change in transcription according to FTY720.

In addition, subtypes of astrocytes were classified astrocyte-enriched single-cell data and spatially visualized (**Supplementary figure 1c**). A total of 5 subtypes of astrocytes were defined, ASC_1 and ASC_3 showed a similar pattern to WM-associated astrocytes. Spatial maps of ASC_5 were similar to that of reactive astrocytes. ASC_2 and ASC_4 cannot be classified into any defined subtype of astrocytes.

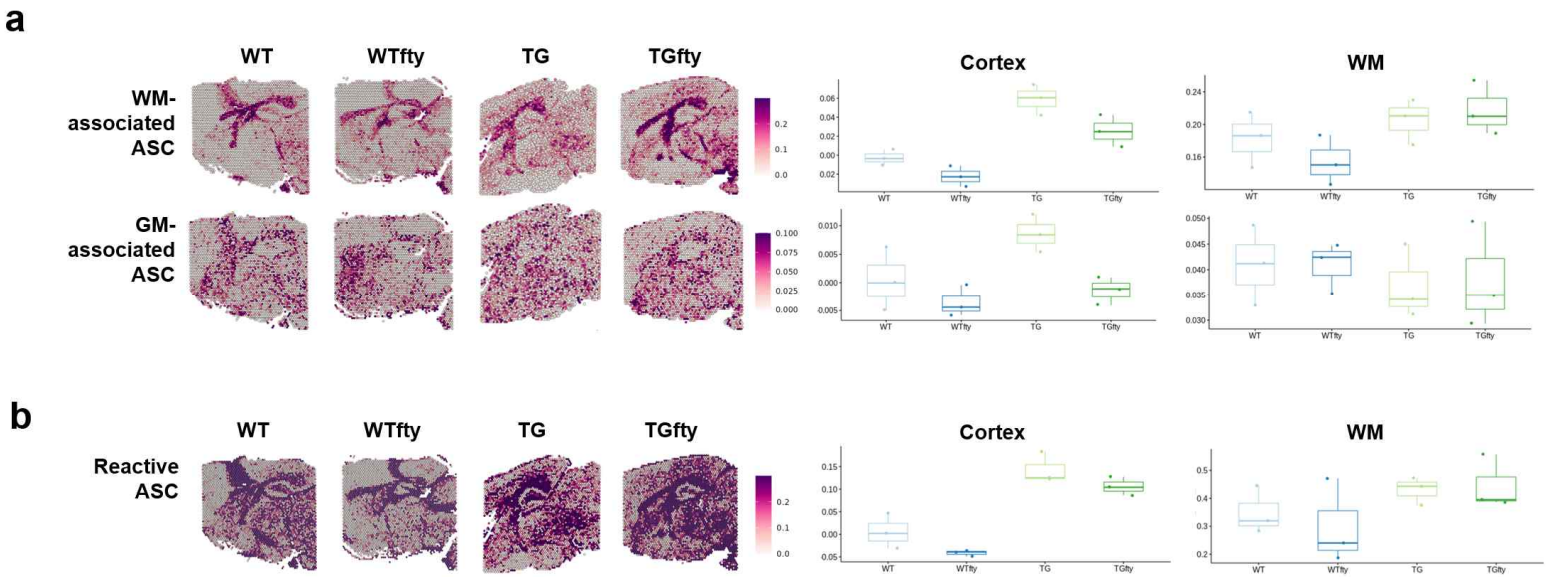


**Figure 12. Spatial map of astrocyte subtypes.** (a) Spatial distribution of WM- and GM-associated astrocytes in sagittal sections. GM-associated astrocyte showed elevated pattern in the cortex of TG, while FTY720 decreased its cortical expression. (b) Spatial distribution of reactive astrocytes. Box and Whisker plots for average fractions of astrocyte subtypes in the cortex and WM. WT: C57BL/6J, WTfty: C57BL/6J with FTY720, TG: 5xFAD, TGfty: 5xFAD with FTY720, ASC: astrocyte.

### 3.4.4. Spatial characteristics of microglia subtypes

The subtypes of microglia were classified based on the marker genes used in the literature (**Table 3**) [52]. Microglia, divided into homeostatic microglia and DAM, were spatially mapped (**Figure 13**). All microglia subtypes showed an increase in the WM, cortex, septum, striatum, and thalamus of TG compared to WT. Spatial maps of microglia subtypes in TG were not changed under FTY720.

Moreover, subtypes of microglia in CD45+ sorted single-cell data were mapped for spatial data (**Supplementary figure 1d**). The spatial map of homeostatic microglia from CD45+ sorted single-cell data was consistent with the spatial map of marker-based homeostatic microglia. The spatial patterns of DAM based on marker genes were similar to the patterns of DAM in CD45+ sorted single-cell data except for WM.

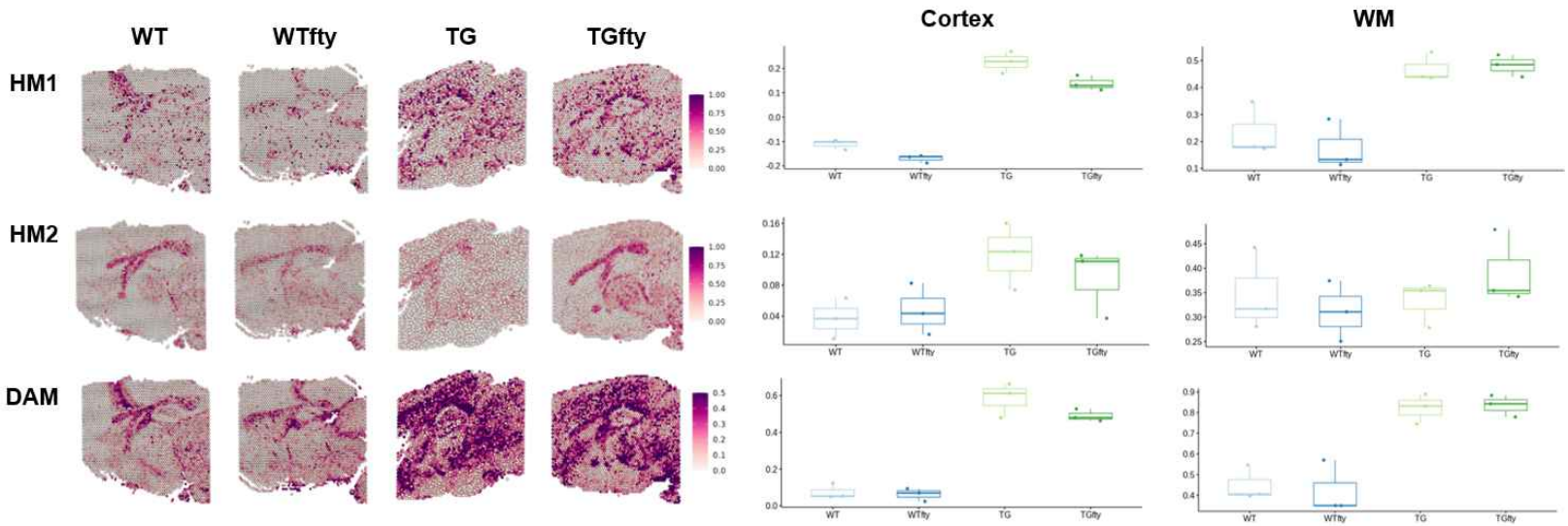


**Figure 13. Spatial map of microglia subtypes.** Spatial distribution of microglia subtypes in sagittal sections. All microglia subtypes were globally increased in TG. Box and Whisker plots for average fractions of microglia subtypes in the cortex and WM. WT: C57BL/6J, WTfty: C57BL/6J with FTY720, TG: 5xFAD, TGfty: 5xFAD with FTY720, HM: homeostatic microglia, DAM: disease-associated microglia.

| Cell type | Marker genes |
|---|---|
| **Astrocytes** | |
| WM-associated ASC | *Lce1m, Ttr, Crlf1, Brinp2, Fbln2, Lce1l, Cldn2, Mag, Mlc1, Vgf, Fabp7, Des, Mbp, Gja5, Scx, Gas7, Vipr2, Aqp4, Nckap1l, Lmln, Cdh2, Nsg2, Fgf2, Sox2, Ltbp1, Gldn, Trf, Esam, Ccl2, Ntrk2, Tbc1d2, Prima1, Vwa1, Plp1, Mt3, Pllp, Prdm16, Itga11, Grem1, Ptgds, Osr2, Ccl7, Bhlhe22, Enpp2, Spink8, Spp1, Ctss, Pcp4l1, Postn, Slc7a8, Lbp, Hopx, C1qc, Pf4, Itga7, Il1rn, Ncf1, C1qb, Cd68, Itga1, Ppp1r14a, Slc30a3, Ankrd37, Tnc, Aif1, Ntm, Bdnf, Mmp12, Eln, Laptm5, Pde2a, Cxcl1, Naaa, Ankrd1, Myh11, Pltp, Il1rl2, Rasl12, Ptgir, Serpine1, Angptl4, Cyfip2, Lyz2, C1qa, Rftn1, Snx30, Tm6sf1, Matn4, Plcl1, S1pr1, Tgm2, Relt, Mtus1, Ralgps2, Svil, Atp8b1, Inpp4b, Inhba, Cfd, Foxs1, Vldlr, Papss2, Il1rl1, Nav3, Hspa1b* |
| GM-associated ASC | *Tmem100, Cldn11, Rspo2, Cdh1, Necab1, Wnt16, Nxn, Ptgfr, Dcaf12l1, Col26a1, Spock3, Ephb2, Pcsk9, Dkk2, Gap43, Pabpc4l, Slc4a10, March11, Mfap5, Bend5, Slc26a7, Tm4sf1, Cdh8, Cpxm2, Clec2d, Tenm4, Nlrp10, Ptgis, Ntrk3, Il18, Avpr1a, Dact2, Ankrd29, Sema5a, Gfra2, Pheta2, Rassf2, Itpr3, Efemp1, Brinp1, Sema3d, Sfrp4, Plagl1, Scd2, Scd, Adrb2, Igfbp4, Zbtb7c, Col9a2, Olfml2a, Rps9, Slc8a1, Gjb2, Myh14, Rasgrp2, Hist1h1a, Thbd, Kit, Penk, Adra2a, E2f2, Slc4a4, Bnc2, Foxd1, Ncor1, Svip, Tk1, Ednra, Rerg, Snai2, Syt1, Myrf* |
| Reactive ASC | *Gfap, Nes, Synm, Vim, Aldoc, Fabp7, Maob, Tspo, Cryab, Hspb1, C3, Chil1, Lcn2, Serpina3n, Mt1, Thbs1, Nfat, Ntrk2, S100b, Sox9, Stat3, Slc1a3, Slc1a2, Kcnj10* |
| **Microglia** | |
| Homeostatic MG1 | *Hexb, Cst3, Sparc, Selplg, P2ry12, Tmem119, Lgmn, Csf1r, Cx3cr1, C1qc, Marcks, C1qa, Serinc3, C1qb, Siglech, Ctss, Olfml3, Gpr34, Cd81* |
| Homeostatic MG2 | *Meg3, Slc1a2, Plp1, Xist, Ubd, Pclo, Snhg11, Fcgbp, Pcdh9, Enpp2, Ptprd, Nrxn3, Apod, S100a16, Sox2ot, Slc24a2, Cntn2, Ank3, Kcna1, Nrxn1, Unc80* |
| DAM | *Ctsb, Ctsd, Cd9, Cst7, Apoe, Ctsz, Tyrobp, Gnas, Ctsl, Cd63, B2m, Lpl, Fth1, Trem2, Lyz2, Cd68, Npc2, Serpine2, AC151602.1* |

**Table 3. Marker genes of astrocyte and microglia subtypes**

WM: white matter, GM: grey matter, ASC: astrocyte, MG: microglia, DAM: disease-associated microglia.

### 3.5 Cell type-specific expression of sphingolipid pathway genes

Cell type-specific expression in spatial transcriptomic data was estimated by DestVI method (**Figure 14**). Genes constituting S1PRs and downstream signaling of S1PRs were evaluated. *S1pr5* was mostly expressed in oligodendrocytes, while the expression of *S1pr1* was mostly covered by astrocytes. The expression levels of *S1pr2*, *S1pr3*, and *S1pr4* in major cells were relatively low compared to *S1pr1* or *S1pr5*. Genes with similar expression patterns were clustered on a heatmap of scaled expression levels: *S1pr5* with *Rac1* and *Spns2*, *S1pr1* with *Ezr*, *S1pr3* with *Pik3cb* and *Akt1*, and *S1pr4* with *Pik3cg*. *S1pr5* and *S1pr1* also showed intergroup differences, which were downregulated in TG but restored by FTY720.

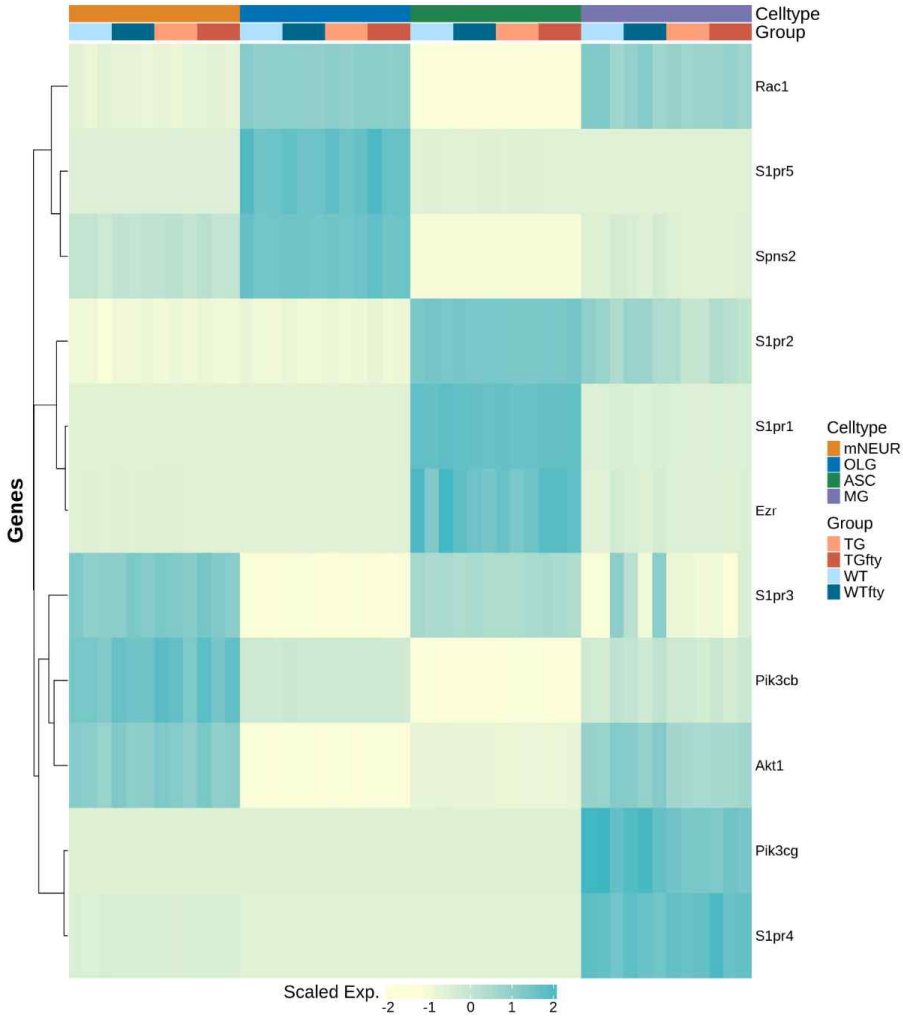


**Figure 14. Heatmap of cell-type specific expression of S1PRs and its downstream pathway genes.** *S1pr1* and *S1pr5* were mainly expressed in astrocyte and oligodendrocyte, respectively. Expression patterns of *Rac1* and *Spns2* were close to that of *S1pr5*. *S1pr1* shared expression patterns with *Ezr*. WT: C57BL/6J, WTfty: C57BL/6J with FTY720, TG: 5xFAD, TGfty: 5xFAD with FTY720, mNEUR: mature neuron, OLG: oligodendrocyte, ASC: astrocyte, MG: microglia.

### 3.6 Correlation of behavior and features of spatial transcriptome

To evaluate the contribution of each spatial transcriptomic feature to the clinical outcome, correlation analyses with the alternation of the Y-maze test were performed. Expressions or cell fractions extracted from representative areas for each feature of spatial transcriptomics were used. Among functional targets of FTY720, *S1pr5* in the WM was positively correlated to the alternation (**Figure 15**). A weak negative correlation was found between the alternation and *S1pr1* in the WM.

The associations between the alternation and the proportion of cell subtypes in the representative areas were also evaluated (**Figure 16**). mfOLG in the WM showed a trend of positive correlation with the alternation, while GLUT in the cortex was negatively correlated to the alternation. No definite correlation was found between DOPA in the VTA and the alternation. The GM-associated astrocyte in the cortex was significantly associated with the alternation.

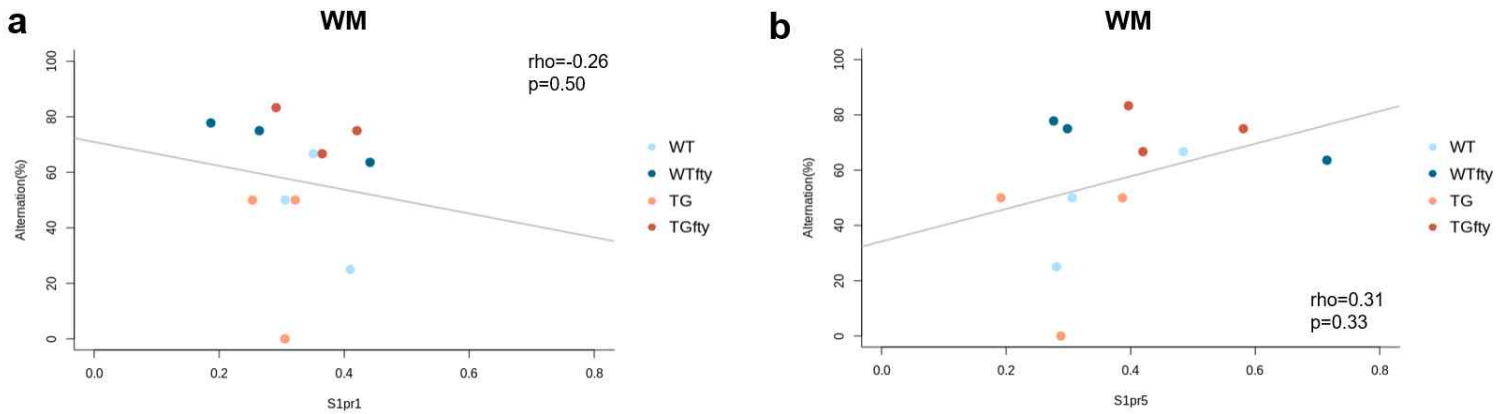


**Figure 15. Correlation between the alternation and S1PRs.** (a) *S1pr1* in the WM showed weak negative correlation with alternation, without statistical significance (rho=-0.26, p=0.50). (b) *S1pr5* in the WM showed positive correlation with alternation, which did not reach statistical significance (rho=0.31, p=0.33). WT: C57BL/6J, WTfty: C57BL/6J with FTY720, TG: 5xFAD, TGfty: 5xFAD with FTY720, WM: white matter.

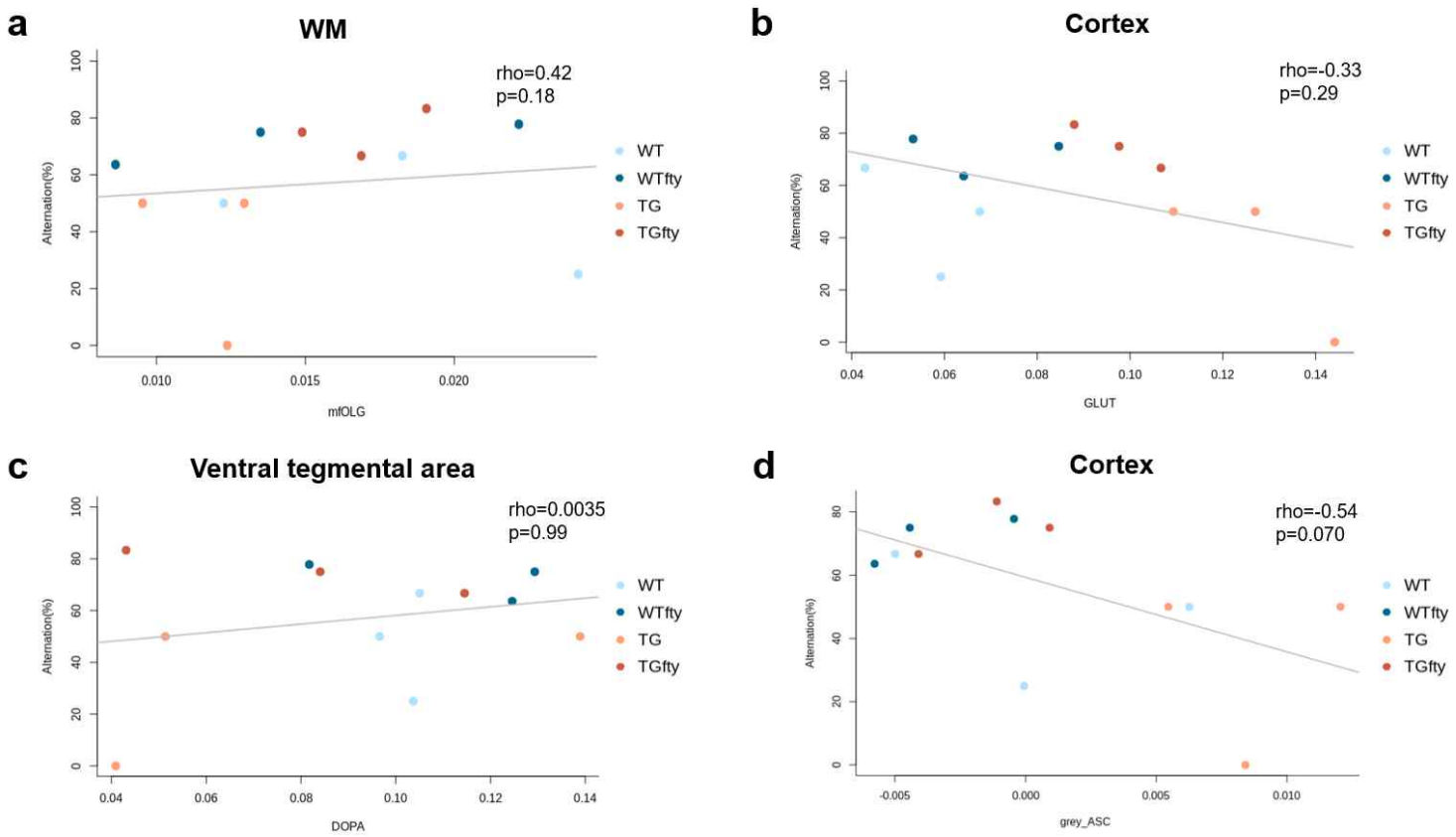
a
WM
rho=0.42
p=0.18
Alternation(%)
mfOLG
WT
WTfty
TG
TGfty
b
Cortex
rho=-0.33
p=0.29
Alternation(%)
GLUT
WT
WTfty
TG
TGfty
c
Ventral tegmental area
rho=0.0035
p=0.99
Alternation(%)
DOPA
WT
WTfty
TG
TGfty
d
Cortex
rho=-0.54
p=0.070
Alternation(%)
grey_ASC
WT
WTfty
TG
TGfty

**Figure 16. Correlation between the alternation and proportion of each cell subtype.** (a) mfOLG in the WM showed positive correlation with the alternation (rho=0.42, p=0.18). (b) Glutamatergic neuron in the cortex showed negative correlation with the alternation (rho=-0.33, p=0.29). (c) Dopaminergic neuron in the ventral tegmental area was weak positively correlated to the alternation (rho=0.0035, p=0.99). (d) GM-associated astrocyte in the cortex showed a significant negative correlation with the alternation (rho=-0.54, p=0.070). WT: C57BL/6J, WTfty: C57BL/6J with FTY720, TG: 5xFAD, TGfty: 5xFAD with FTY720, mfOLG: myeline-forming oligodendrocyte, GLUT: glutamatergic neuron, DOPA; dopaminergic neuron, grey_ASC: GM-associated astrocyte, WM: white matter.

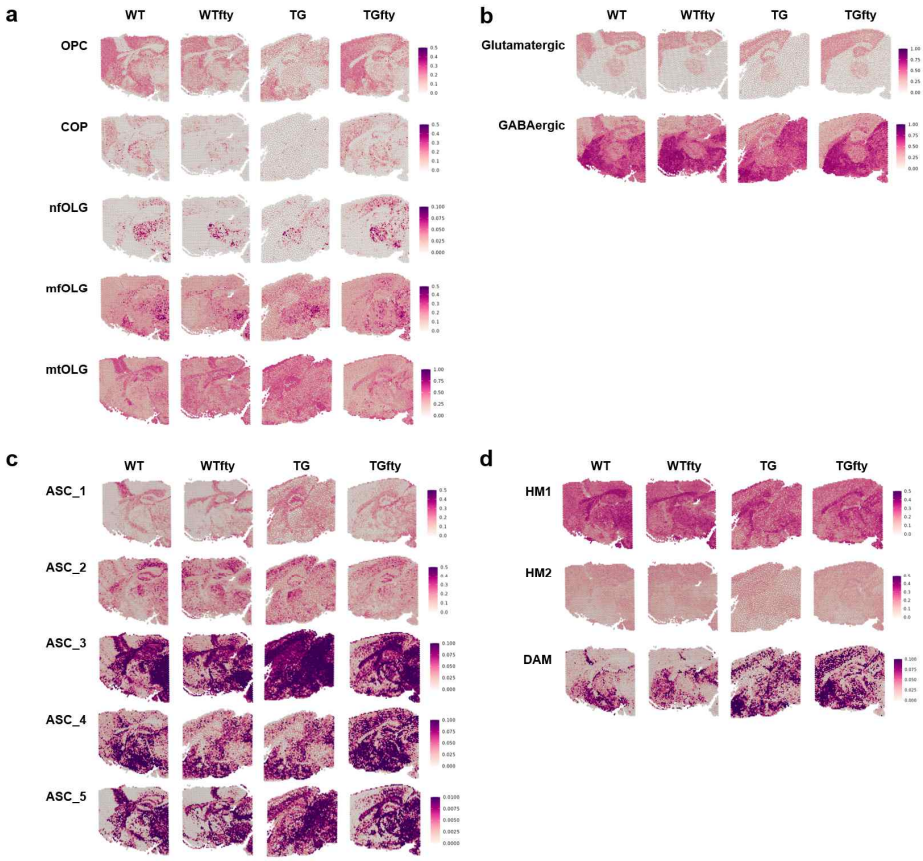


**Supplementary figure 1. Spatial map of cell subtypes from public single-cell RNA sequencing.** (a) Spatial patterns of oligodendrocyte lineage cells from oligodendrocyte-enriched single-cell data. (b) Spatial patterns of excitatory and inhibitory neurons from neuron-enriched single-cell data. (c) Spatial patterns of astrocyte subtypes from astrocyte-enriched single-cell data. (d) Spatial patterns of microglia subtypes from CD45+ enriched single-cell data. WT: C57BL/6J, WTfty: C57BL/6J with FTY720, TG: 5xFAD, TGfty: 5xFAD with FTY720, OPC: oligodendrocyte precursor cell, COP: differentiation-committed oligodendrocyte precursor, nfOLG: newly formed oligodendrocyte, mfOLG: myeline-forming oligodendrocyte, mtOLG: mature oligodendrocyte, ASC: astrocyte, HM: homeostatic microglia, DAM: disease associated microglia.

# 4. Discussion

The spatial mapping enables us to understand of the effects and mechanisms of the brain-targeted drugs through area-specific patterns. In addition, the composition of brain cells and their correlation with spatial patterns can be analyzed by integrating single-cell data with the spatial transcriptome.

Behavioral change that partially represents memory change was observed after FTY720 treatment. To evaluate whether FTY720 directly influences brain cells in which area and to which brain cells, the FTY720-related changes in the regional distribution of brain cells were mainly focused. Gene ontology analyses on spatial transcriptome and WGCNA modules helped to predict the major cell type in the WM as oligodendrocytes and in the cortex and striatum as neuronal lineage cells. The cellular composition of the spatial spot was analyzed by integration of public single-cell data with spatial data. Oligodendrocyte showed characteristic patterns in the WM according to FTY720, while the spatial distributions of neuron were similar among groups. Spatial changes in subtypes of neuronal lineage cells by FTY720 were also observed. Moreover, glial cells including astrocytes and microglia were spatially mapped according to their subtypes. In addition to visual assessment of

spatial maps, quantitative analyses were performed for each cell subtype in each representative area. Finally, correlations between the behavior and each feature of spatial transcriptome were assessed to discover the possible therapeutic target of FTY720.

### 4.1 Effects of FTY720 unraveled by spatial transcriptome

Owing to the absence of notable findings in the hippocampus, a classical susceptible region of AD [69], the area where FTY720 actions were focused. The pharmacological target of FTY720 is S1PRs, and spatial maps of S1PRs showed subtype-specific patterns. *S1pr1* was widely distributed, while *S1pr5* was centered on the WM. S1PR1 is expressed in neurons, astrocytes, oligodendrocytes, and microglia, while S1PR5 is abundant in oligodendrocytes, microglia, and astrocytes [70]. FTY720 enhanced WM-specific transcription of *S1pr1*, *S1pr5*, and genes constituting the downstream pathway of S1PRs in the WM. Since FTY720 is known to antagonize S1PRs in CNS [17], these results matched with the expected overexpression of *S1pr1* and *S1pr5* due to downregulation by FTY720. In vivo study that showed the modulation of genes related to sphingolipid metabolism by FTY720 in APP LD2/B6 AD model mice supports this finding [71]. FTY720 induces the transcription of S1PRs mainly targeting the WM. In addition, the

association of S1PRs in the WM with the behavior outcome was analyzed. *S1pr5* in the WM showed a positive correlation with the alternation, although statistical significance was not reached. To summarize, the enhanced expression of *S1pr5* in the WM by FTY720 could be related to behavior improvement.

WGCNA was also performed to specify the brain region where differences in transcriptome between groups. The pink module was spatially restricted to the WM and showed a strong correlation with oligodendrocyte. The blue module was spatially presented on the cortex and hippocampus and correlated with mature neuron and OPC. FTY720 influenced the transcriptome of oligodendrocyte lineage cells in the WM of TG and glutamatergic neurons in the cortex of TG. This shows how appropriate the WGCNA is for selecting the direction of further analysis.

**4.2 Comprehensive analysis of the cell type-specific effect of FTY720**

Spatial patterns of major cell types in the brain were characterized by integrative analysis of the single-cell data and spatial transcriptome. Oligodendrocyte presented a distinctive spatial pattern that spreads from WM to the adjacent deeper layer of cortex and striatum in TG, but is rather limited to WM after FTY720 treatment. On the contrary, neuron showed a consistent pattern among groups. Astrocytes and microglia

were both diffusely distributed in TG, however, no effect of FTY720 was observed.

To discover the spatial changes in the subtypes of oligodendrocyte, additional analysis by subtyping of oligodendrocyte lineage cells based on the markers from literature was performed. Each oligodendrocyte lineage cell including OPC, nfOLG, mfOLG, and mtOLG showed a characteristic spatial map under FTY720 treatment. Although nfOLG and mfOLG showed increased fractions in the WM, thalamus, and cortex, FTY720 only reversed the spatial pattern of mfOLG in the WM. OPC and mtOLG remained constantly among groups. There was a slight discrepancy between spatial maps of nfOLG, mfOLG, and mtOLG according to the used data form. These unmatched patterns could be result from mislabeling of the small cell population or misprediction of the fractions from the enriched cell population. Oligodendrocytes in CNS are responsible for myelin production, and sequentially mature from OPC to COP, nfOLG, mfOLG, and finally to mtOLG. Under neurodegenerative status, FTY720 appeared to encourage transcription of premature oligodendrocyte lineage cells in the WM. Literature suggests that FTY720 promoted proliferation and differentiation of OPC in EAE and demyelination models [72, 73]. It has been also demonstrated that FTY720 promoted axonal integrity and

reduction of demyelination in the WM [74]. The spatial transcriptional results are compatible with the indicated role for FTY720 on oligodendrocyte lineage cells of the WM in neurodegenerative conditions. The clinical result of the positive contribution of FTY720 to oligodendrocyte lineage cells in the WM of TG was also evaluated. An increased fraction of mfOLG was related to the enhanced alternation, which statistical significance was not achieved. The mfOLG in the WM could be suggested as a possible therapeutic target of FTY720.

Spatial maps of subtypes of neuronal lineage cells were also visualized. Subtypes including NRP, ImmN, GABAergic neuron, and NendC were consistent among groups. The estimated fraction of cholinergic neurons was too small that the interpretation of the spatial patterns was limited. Glutamatergic neurons showed increased fraction in the cortex of TG, while FTY720 decreased its fraction. No other areas in the brain had transcriptional change of glutamatergic neurons according to FTY720. Glutamate, a neurotransmitter used for glutamatergic neurons, is also a neurotoxin that has been implicated as one of the pathogenesis of AD [75]. Glutamatergic neurons and glial cells compose tight regulation of glutamate through the glutamate-glutamine cycle [76]. Excess glutamate in the synaptic cleft can causing excitotoxicity to glutamatergic neurons by leading to the influx of $Ca^{2+}$

and eventually cause neuronal death [77]. Since maintenance of a stable state of glutamatergic neurons is crucial for brain homeostasis, efforts to reduce the excitation of glutamatergic neuron has been extensively studied [78]. Hence, the effect of FTY720 restricting the transcription of the glutamatergic neurons in the cortex is noteworthy. Moreover, the fraction of glutamatergic neurons in the cortex and behavior were confirmed to be negatively correlated. Thus, FTY720 the drug that can restrict the glutamatergic neuron in the cortex can be considered a contributable factor to the improvement of behavior. The transcription of dopaminergic neurons in TG was influenced by FTY720 in the VTA. Dopaminergic neurons in the VTA follow the mesocorticolimbic pathway, which projects to the striatum, limbic system, and prefrontal cortex [79]. The degeneration of dopaminergic neurons in the VTA contributes to memory decline in the AD model [80]. Pharmacological treatments targeting the dopaminergic system have been suggested for AD [81]. However, no association was found between the alternation and the fraction of dopaminergic neurons in the VTA. As the correlation result shows, the glutamatergic neurons in the cortex have the potential to be an actual therapeutic target of FTY720.

Subtype-specific spatial patterns of glial cells including astrocytes were also confirmed. Regardless of the astrocyte subtype, TG

showed an increased pattern of astrocytes in areas covering the cortex, septum, striatum, and thalamus. GM-associated astrocytes were downregulated in the cortex by FTY720. In GM, astrocytes are exposed to high glutamate from numerous glutamatergic neurons, and lead to enhanced glutamate clearance in the synaptic cleft [82]. As glutamatergic neurons and astrocytes are closely connected [83], the transcriptional inhibition by FTY720 to the glutamatergic neurons may influence the transcription of the GM-associated astrocyte. In fact, the downregulation of GM-associated astrocytes in the cortex was significantly correlated to behavior improvement. Thus, along with the glutamatergic neurons, GM-associated astrocytes in the cortex can be a suggested target of FTY720 that result in clinical outcomes. FTY720-induced transcriptional changes in the WM, septum, striatum, and thalamus were not found in both GM-associated astrocyte and WM-associated astrocyte. Compatible with the recent studies suggesting prolonged activation of astrocytes contributes to AD pathology [84], reactive astrocytes showed increased transcription in TG. Reactive astrocytes are known to respond to the amyloid beta [85], and the increased deposition of amyloid beta in the TG was consistent with spatial transcriptomics of reactive astrocyte. Moreover, consistent deposition of amyloid beta after FTY720 was also matched with consistent spatial patterns of reactive astrocyte by FTY720.

Moreover, each subtype of microglia was spatially distributed and the effect of FTY720 on microglia was confirmed. Spatial patterns of both homeostatic microglia and DAM were diffusely spread in TG, however, no change was found under FTY720 treatment. In addition, spatial transcriptomics of microglia subtypes was not correlated to the behavior. DAM, a subtype of microglia with enhanced phagocytic activity and increased lipid metabolism, is found to be localized near the amyloid plaques [52]. Consistent fluorescence of amyloid beta between TG and TG with FTY720 was correlated with spatial maps of DAM that showed no change according to the FTY720 treatment.

### 4.3 Limitations

Although intensive analyses on spatial transcriptomic data were performed, there are some limitations. First, the number of mouse tissue samples per group was small, and subtle variations in slice position for each mouse were inevitable. The genetic information from spatial data can be misinterpreted when the slide sections are mismatched. Therefore, additional tissue samples in sagittal sections will be necessary to confirm the results of transcriptomic change in the spatial map. Moreover, the age of enrolled mice was too old that the behavioral difference between the WT and TG was not significant. Using mice of younger age but old

enough to express AD pathology would help to verify the difference in clinical outcomes between WT and TG.

Public single-cell data consisted of various groups of mice. Although the selection of brain cell markers is based on genes with low variations among different model mice, the spatial pattern of TG should be carefully examined. To overcome the underlying variation between WT and TG, integrative analyses composed of single-cell sequencing of TG should be further included.

### 4.4 Future directions

The integrative analysis of single-cell sequencing and spatial transcriptome in the brain could be used for the development of drugs, especially for drugs targeting neurological effects. Since the brain is a complex organ in which made of various cells, the pharmacological effect of a drug is too difficult to interpret in fragmented studies. A comprehensive method including sequencing and spatial transcriptomics data can provide insights into drug developers and clinicians since transcriptomic changes can be shown on the spatial map of brain cells. Moreover, this could be used to find and specify new targets for drugs and to screen for the pathways involved.

Confirmation of transcriptomic data in detail should be added to strengthen the results. Although gene expression is dependent on transcription, transcriptional abundance may not always correlate with the action of gene product due to various regulations after the transcription. Thus, caution needs to be exerted in interpreting the transcriptomic data. FTY720 has been found to influence the transcriptomics of glutamatergic neurons and dopaminergic neurons, and evaluation of neurotransmitter levels can be used as one of the methods to confirm neuronal function. For in vivo measurements of neurotransmitters, microdialysis that detects the target with high selectivity and sensitivity can be suggested [86]. Noninvasive imaging biomarkers using F-18 FTY720 PET integrated with transcriptomic data could clarify the area-specific transcriptomic changes by FTY720. In addition, investigation of periphery organs including lymph nodes, liver, and spleen using spatial transcriptomic data should be further considered to identify the role of FTY720 in the relationship between the peripheral immune system and the CNS.

# 5. Conclusion

FTY720, a potential drug for AD, induced cell type-specific transcriptomic change in each representative area. The upregulation of *S1pr5*, the target of FTY720, in the WM was correlated with behavior improvement. The spatial pattern of oligodendrocyte in myelin-forming state was WM-restricted, which also had a positive correlation to the clinical outcome. Moreover, downregulation of glutamatergic neurons and GM-associated astrocytes in the cortex by FTY720 was associated with good performance. Dopaminergic neurons in the ventral tegmental area were upregulated by FTY720, however, no clinical association was found. Integrative analysis of single-cell sequencing and spatial transcriptomics suggested the potential area-specific targets of FTY720 in the brain. Thus, it can be a promising method to understand the area-specific and cell type-specific action of CNS drugs.

# References


1. Butters, N., D.C. Delis, and J.A. Lucas, *Clinical assessment of memory disorders in amnesia and dementia.* Annual Review of Psychology, 1995. **46**(1): p. 493-523.
2. Guzior, N., et al., *Recent development of multifunctional agents as potential drug candidates for the treatment of Alzheimer's disease.* Current medicinal chemistry, 2015. **22**(3): p. 373-404.
3. Sanabria-Castro, A., I. Alvarado-Echeverría, and C. Monge-Bonilla, *Molecular pathogenesis of Alzheimer's disease: an update.* Annals of neurosciences, 2017. **24**(1): p. 46-54.
4. Corbett, A., et al., *Drug repositioning for Alzheimer's disease.* Nature Reviews Drug Discovery, 2012. **11**(11): p. 833-846.
5. Hodos, R.A., et al., *In silico methods for drug repurposing and pharmacology.* Wiley Interdisciplinary Reviews: Systems Biology and Medicine, 2016. **8**(3): p. 186-210.
6. Zhang, M., et al., *Drug repositioning for Alzheimer's disease based on systematic 'omics' data mining.* PloS one, 2016. **11**(12): p. e0168812.
7. Kappos, L., et al., *Oral fingolimod (FTY720) for relapsing multiple sclerosis.* New England Journal of Medicine, 2006.

**355**(11): p. 1124-1140.

8. Kappos, L., et al., *A placebo-controlled trial of oral fingolimod in relapsing multiple sclerosis.* New England Journal of Medicine, 2010. **362**(5): p. 387-401.

9. Brinkmann, V., et al., *The immune modulator FTY720 targets sphingosine 1-phosphate receptors.* Journal of Biological Chemistry, 2002. **277**(24): p. 21453-21457.

10. Gräler, M.H. and E.J. Goetzl, *The immunosuppressant FTY720 down-regulates sphingosine 1-phosphate G protein-coupled receptors.* The FASEB journal, 2004. **18**(3): p. 551-553.

11. Mandala, S., et al., *Alteration of lymphocyte trafficking by sphingosine-1-phosphate receptor agonists.* Science, 2002. **296**(5566): p. 346-349.

12. Fujino, M., et al., *Amelioration of experimental autoimmune encephalomyelitis in Lewis rats by FTY720 treatment.* Journal of Pharmacology and Experimental Therapeutics, 2003. **305**(1): p. 70-77.

13. Rausch, M., et al., *Predictability of FTY720 efficacy in experimental autoimmune encephalomyelitis by in vivo macrophage tracking: clinical implications for ultrasmall superparamagnetic iron oxide-enhanced magnetic resonance*

*imaging.* Journal of Magnetic Resonance Imaging: An Official Journal of the International Society for Magnetic Resonance in Medicine, 2004. **20**(1): p. 16-24.

14. Foster, C.A., et al., *Brain penetration of the oral immunomodulatory drug FTY720 and its phosphorylation in the central nervous system during experimental autoimmune encephalomyelitis: consequences for mode of action in multiple sclerosis.* Journal of Pharmacology and Experimental Therapeutics, 2007. **323**(2): p. 469-475.

15. Meno-Tetang, G.M., et al., *Physiologically based pharmacokinetic modeling of FTY720 (2-amino-2 [2-(-4-octylphenyl) ethyl] propane-1, 3-diol hydrochloride) in rats after oral and intravenous doses.* Drug metabolism and disposition, 2006. **34**(9): p. 1480-1487.

16. Shaikh, R.S., et al., *Synthesis and evaluation of fluorinated fingolimod (FTY720) analogues for sphingosine-1-phosphate receptor molecular imaging by positron emission tomography.* Journal of Medicinal Chemistry, 2015. **58**(8): p. 3471-3484.

17. Brinkmann, V., *Sphingosine 1-phosphate receptors in health and disease: mechanistic insights from gene deletion studies and reverse pharmacology.* Pharmacology & therapeutics, 2007.

**115**(1): p. 84-105.

18. Jaillard, C., et al., *Edg8/S1P5: an oligodendroglial receptor with dual function on process retraction and cell survival.* Journal of Neuroscience, 2005. **25**(6): p. 1459-1469.

19. Kimura, A., et al., *Essential roles of sphingosine 1-phosphate/S1P1 receptor axis in the migration of neural stem cells toward a site of spinal cord injury.* Stem cells, 2007. **25**(1): p. 115-124.

20. Wu, Y.-P., et al., *Sphingosine kinase 1/S1P receptor signaling axis controls glial proliferation in mice with Sandhoff disease.* Human molecular genetics, 2008. **17**(15): p. 2257-2264.

21. Hunter, S.F., J.D. Bowen, and A.T. Reder, *The direct effects of fingolimod in the central nervous system: implications for relapsing multiple sclerosis.* CNS drugs, 2016. **30**(2): p. 135-147.

22. He, X., et al., *Deregulation of sphingolipid metabolism in Alzheimer's disease.* Neurobiology of aging, 2010. **31**(3): p. 398-408.

23. Mielke, M.M. and C.G. Lyketsos, *Alterations of the sphingolipid pathway in Alzheimer's disease: new biomarkers and treatment targets?* Neuromolecular medicine, 2010. **12**(4): p. 331-340.

24. Carreras, I., et al., *Dual dose-dependent effects of fingolimod in*

*a mouse model of Alzheimer's disease.* Scientific reports, 2019. **9**(1): p. 1-11.

25. Aytan, N., et al., *Fingolimod modulates multiple neuroinflammatory markers in a mouse model of Alzheimer's disease.* Scientific reports, 2016. **6**(1): p. 1-9.

26. Squire, L.R., *Memory and the hippocampus: a synthesis from findings with rats, monkeys, and humans.* Psychological review, 1992. **99**(2): p. 195.

27. Li, Y., Y. Mu, and F.H. Gage, *Development of neural circuits in the adult hippocampus.* Current topics in developmental biology, 2009. **87**: p. 149-174.

28. Stoub, T.R., et al., *Hippocampal disconnection contributes to memory dysfunction in individuals at risk for Alzheimer's disease.* Proceedings of the National Academy of Sciences, 2006. **103**(26): p. 10041-10045.

29. Végh, M.J., et al., *Reducing hippocampal extracellular matrix reverses early memory deficits in a mouse model of Alzheimer's disease.* Acta neuropathologica communications, 2014. **2**(1): p. 1-11.

30. Bartzokis, G., *Alzheimer's disease as homeostatic responses to age-related myelin breakdown.* Neurobiology of aging, 2011.

**32**(8): p. 1341-1371.

31. Brun, A. and E. Englund, *A white matter disorder in dementia of the Alzheimer type: a pathoanatomical study.* Annals of neurology, 1986. **19**(3): p. 253-262.

32. Englund, E., A. Brun, and C. Alling, *White matter changes in dementia of Alzheimer's type: biochemical and neuropathological correlates.* Brain, 1988. **111**(6): p. 1425-1439.

33. Menn, B., et al., *Origin of oligodendrocytes in the subventricular zone of the adult brain.* Journal of Neuroscience, 2006. **26**(30): p. 7907-7918.

34. Behrendt, G., et al., *Dynamic changes in myelin aberrations and oligodendrocyte generation in chronic amyloidosis in mice and men.* Glia, 2013. **61**(2): p. 273-286.

35. Gagyi, E., et al., *Decreased oligodendrocyte nuclear diameter in Alzheimer's disease and Lewy body dementia.* Brain Pathology, 2012. **22**(6): p. 803-810.

36. Kapfhammer, J. and M.E. Schwab, *Inverse patterns of myelination and GAP-43 expression in the adult CNS: neurite growth inhibitors as regulators of neuronal plasticity?* Journal of Comparative Neurology, 1994. **340**(2): p. 194-206.

37. Kelleher, R.J. and J. Shen, *Presenilin-1 mutations and*

*Alzheimer's disease.* Proceedings of the National Academy of Sciences, 2017. **114**(4): p. 629-631.

38. Holt, C.E., K.C. Martin, and E.M. Schuman, *Local translation in neurons: visualization and function.* Nature structural & molecular biology, 2019. **26**(7): p. 557-566.

39. Crews, L. and E. Masliah, *Molecular mechanisms of neurodegeneration in Alzheimer's disease.* Human molecular genetics, 2010. **19**(R1): p. R12-R20.

40. Perlson, E., et al., *Retrograde axonal transport: pathways to cell death?* Trends in neurosciences, 2010. **33**(7): p. 335-344.

41. Terry, R.D., et al., *Physical basis of cognitive alterations in Alzheimer's disease: synapse loss is the major correlate of cognitive impairment.* Annals of Neurology: Official Journal of the American Neurological Association and the Child Neurology Society, 1991. **30**(4): p. 572-580.

42. DeKosky, S.T. and S.W. Scheff, *Synapse loss in frontal cortex biopsies in Alzheimer's disease: correlation with cognitive severity.* Annals of Neurology: Official Journal of the American Neurological Association and the Child Neurology Society, 1990. **27**(5): p. 457-464.

43. McKenzie, I.A., et al., *Motor skill learning requires active*

*central myelination.* science, 2014. **346**(6207): p. 318-322.

44. Avila-Muñoz, E. and C. Arias, *When astrocytes become harmful: functional and inflammatory responses that contribute to Alzheimer's disease.* Ageing research reviews, 2014. **18**: p. 29-40.

45. Verkhratsky, A., et al., *Astrocytes in Alzheimer's disease.* Neurotherapeutics, 2010. **7**(4): p. 399-412.

46. Rodriguez, J., et al., *Astroglia in dementia and Alzheimer's disease.* Cell Death & Differentiation, 2009. **16**(3): p. 378-385.

47. Liddelow, S.A., et al., *Neurotoxic reactive astrocytes are induced by activated microglia.* Nature, 2017. **541**(7638): p. 481-487.

48. Miller, R.H. and M.C. Raff, *Fibrous and protoplasmic astrocytes are biochemically and developmentally distinct.* Journal of Neuroscience, 1984. **4**(2): p. 585-592.

49. Escartin, C., et al., *Reactive astrocyte nomenclature, definitions, and future directions.* Nature neuroscience, 2021. **24**(3): p. 312-325.

50. Sierra, A., et al., *Microglia shape adult hippocampal neurogenesis through apoptosis-coupled phagocytosis.* Cell stem cell, 2010. **7**(4): p. 483-495.

51. Hickman, S.E., E.K. Allison, and J. El Khoury, *Microglial dysfunction and defective β-amyloid clearance pathways in aging*

*Alzheimer's disease mice.* Journal of Neuroscience, 2008. **28**(33): p. 8354-8360.

52. Keren-Shaul, H., et al., *A unique microglia type associated with restricting development of Alzheimer's disease.* Cell, 2017. **169**(7): p. 1276-1290. e17.

53. Larsson, L., J. Frisén, and J. Lundeberg, *Spatially resolved transcriptomics adds a new dimension to genomics.* Nature Methods, 2021. **18**(1): p. 15-18.

54. Ståhl, P.L., et al., *Visualization and analysis of gene expression in tissue sections by spatial transcriptomics.* Science, 2016. **353**(6294): p. 78-82.

55. Kleshchevnikov, V., et al., *Cell2location maps fine-grained cell types in spatial transcriptomics.* Nature biotechnology, 2022: p. 1-11.

56. Stuart, T., et al., *Comprehensive integration of single-cell data.* Cell, 2019. **177**(7): p. 1888-1902. e21.

57. Center for drug evaluation and research, F., *Parmacology Review.* FDA.

58. Lein, E.S., et al., *Genome-wide atlas of gene expression in the adult mouse brain.* Nature, 2007. **445**(7124): p. 168-176.

59. Yu, G., et al., *clusterProfiler: an R package for comparing*

*biological themes among gene clusters.* Omics: a journal of integrative biology, 2012. **16**(5): p. 284-287.

60. Ximerakis, M., et al., *Single-cell transcriptomic profiling of the aging mouse brain.* Nature neuroscience, 2019. **22**(10): p. 1696-1708.

61. Marques, S., et al., *Oligodendrocyte heterogeneity in the mouse juvenile and adult central nervous system.* Science, 2016. **352**(6291): p. 1326-1329.

62. Yao, Z., et al., *A taxonomy of transcriptomic cell types across the isocortex and hippocampal formation.* Cell, 2021. **184**(12): p. 3222-3241. e26.

63. Batiuk, M.Y., et al., *Identification of region-specific astrocyte subtypes at single cell resolution.* Nature communications, 2020. **11**(1): p. 1-15.

64. Aevermann, B., et al., *A machine learning method for the discovery of minimum marker gene combinations for cell type identification from single-cell RNA sequencing.* Genome research, 2021. **31**(10): p. 1767-1780.

65. Bae, S., et al., *CellDART: cell type inference by domain adaptation of single-cell and spatial transcriptomic data.* Nucleic Acids Research, 2022.

66. Lopez, R., et al., *DestVI identifies continuums of cell types in spatial transcriptomics data.* Nature biotechnology, 2022: p. 1-10.

67. Gokce, O., et al., *Cellular taxonomy of the mouse striatum as revealed by single-cell RNA-seq.* Cell reports, 2016. **16**(4): p. 1126-1137.

68. Werkman, I.L., et al., *Transcriptional heterogeneity between primary adult grey and white matter astrocytes underlie differences in modulation of in vitro myelination.* Journal of neuroinflammation, 2020. **17**(1): p. 1-18.

69. Jack, C.R., et al., *Rate of medial temporal lobe atrophy in typical aging and Alzheimer's disease.* Neurology, 1998. **51**(4): p. 993-999.

70. Aktas, O., et al., *Fingolimod is a potential novel therapy for multiple sclerosis.* Nature Reviews Neurology, 2010. **6**(7): p. 373-382.

71. Jęśko, H., et al., *Modulatory effects of fingolimod (FTY720) on the expression of sphingolipid metabolism-related genes in an animal model of Alzheimer's disease.* Molecular neurobiology, 2019. **56**(1): p. 174-185.

72. Zhang, J., et al., *Fingolimod treatment promotes proliferation*

*and differentiation of oligodendrocyte progenitor cells in mice with experimental autoimmune encephalomyelitis.* Neurobiology of Disease, 2015. **76**: p. 57-66.

73. Yazdi, A., et al., *Fingolimod enhances oligodendrocyte differentiation of transplanted human induced pluripotent stem cell-derived neural progenitors.* Iranian Journal of Pharmaceutical Research: IJPR, 2018. **17**(4): p. 1444.

74. Gurevich, M., et al., *Fingolimod-improved axonal and myelin integrity of white matter tracts associated with multiple sclerosis-related functional impairments.* CNS neuroscience & therapeutics, 2018. **24**(5): p. 412-419.

75. Greenamyre, J.T., et al., *Glutamate transmission and toxicity in Alzheimer's disease.* Progress in Neuro-Psychopharmacology and Biological Psychiatry, 1988. **12**(4): p. 421-IN4.

76. Hertz, L., *Functional interactions between neurons and astrocytes I. Turnover and metabolism of putative amino acid transmitters.* Progress in neurobiology, 1979. **13**(3): p. 277-323.

77. Jacob, C., et al., *Alterations in expression of glutamatergic transporters and receptors in sporadic Alzheimer's disease.* Journal of Alzheimer's Disease, 2007. **11**(1): p. 97-116.

78. Riedel, G., B. Platt, and J. Micheau, *Glutamate receptor function*

*in learning and memory.* Behavioural brain research, 2003. **140**(1-2): p. 1-47.

79. Luo, S.X. and E.J. Huang, *Dopaminergic neurons and brain reward pathways: from neurogenesis to circuit assembly.* The American journal of pathology, 2016. **186**(3): p. 478-488.

80. Nobili, A., et al., *Dopamine neuronal loss contributes to memory and reward dysfunction in a model of Alzheimer's disease.* Nature communications, 2017. **8**(1): p. 1-14.

81. Pan, X., et al., *Dopamine and dopamine receptors in Alzheimer's disease: a systematic review and network meta-analysis.* Frontiers in aging neuroscience, 2019. **11**: p. 175.

82. Köhler, S., U. Winkler, and J. Hirrlinger, *Heterogeneity of astrocytes in grey and white matter.* Neurochemical Research, 2021. **46**(1): p. 3-14.

83. Parpura, V., et al., *Glutamate-mediated astrocyte–neuron signalling.* Nature, 1994. **369**(6483): p. 744-747.

84. Cai, Z., C.-Q. Wan, and Z. Liu, *Astrocyte and Alzheimer's disease.* Journal of neurology, 2017. **264**(10): p. 2068-2074.

85. Allaman, I., et al., *Amyloid-β aggregates cause alterations of astrocytic metabolic phenotype: impact on neuronal viability.* Journal of Neuroscience, 2010. **30**(9): p. 3326-3338.

86. Chefer, V.I., et al., *Overview of brain microdialysis.* Current protocols in neuroscience, 2009. **47**(1): p. 7.1. 1-7.1. 28.

# 국문 초록

## 공간 전사체학으로 밝힌
## FTY720의 알츠하이머병 쥐의 뇌에 미치는 영향

서훈녕

분자의학 및 바이오제약학과

서울대학교 융합과학기술대학원

알츠하이머병과 같은 신경퇴행성질환은 아직까지 명확한 치료제가 없으며 치료제의 개발 과정에 많은 노력이 든다. 최근 빠른 임상 응용이 가능한 기존 FDA의 허가를 받은 약제들을 다른 질환에 적응하는 방법이 제시되고 있다. 이에 FTY720 (fingolimod)라는 FDA의 승인을 받은 재발성 다발성 경화증 약제의 알츠하이머병에 응용 가능성이 대두되었다. 기존에 FTY720가 알츠하이머병 동물 모델의 뇌에 미치는 영향에 대한 연구들이 진행되었으나 뇌세포와 뇌 영역별 다양성을 고려하지 않아 FTY720의 효과를 분석하기에 제한적이다.

본 연구에서는 FTY720을 0.3 mg/kg/일 농도로 7주간 경구 투여한 7개월령 쥐 모델의 뇌로부터 얻은 공간 전사체 데이터를 분석하였다. 행동실험에서 5xFAD 알츠하이머병 모

델 쥐의 행동 저하는 FTY720에 의해 회복되었다. 아밀로이드 베타의 뇌내 축적은 5xFAD 알츠하이머병 모델 쥐에서 전반적으로 증가했으나 FTY720에 의해 변하지 않았다. FTY720 투여에 따라 FTY720의 표적수용체인 S1PR들은 백질에서의 전사체 변화를 특징적으로 보였다. 이와 함께 유전자 공발현 분석 (weighted gene co-expression network analysis)으로 백질과 대뇌피질에 특징적으로 발현하는 모듈의 희돌기아교세포 및 신경세포와의 연관성을 확인하였다.

또한, 공간 전사체 데이터와 공공 단일 세포 전사체 데이터를 NS-Forest (Necessary and Sufficient Forest) 또는 CellDART 방법을 사용하여 통합 분석하였다. 세포 유형별 공간 지도를 작성하였고, 희돌기아교세포에서 FTY720에 의한 백질 중심의 공간 분포의 변화가 두드러졌다. 백질의 수초형성 희돌기아교세포가 FTY720로 전사체가 증가했으며 이는 행동의 호전과 관련성을 보였다. 대뇌피질의 글루탐산신경세포와 회백질연관성상세포는 공통적으로 5xFAD 알츠하이머병 모델 쥐에서 증가하였으나 FTY720에 의해 감소되었고, 행동 호전과 상관성을 보였다. 도파민성신경세포는 복측피개야에서 FTY720에 의한 전사체 증가가 관찰됐으나 행동과의 상관성은 없었다.

FTY720은 5xFAD 알츠하이머병 모델 쥐의 백질에서 표적수용체의 전사를 증가시켰으며, 이는 백질에서의 수초형성 희돌기아교세포의 상향 조절과 함께 나타났다. 더불어 회백질의 글루탐산신경세포와 회백질연관성상세포는 FTY720에 의

한 유사한 공간 전사체 패턴을 보였다. 정리하면 FTY720이 백질의 수초형성 희돌기아교세포의 전사체 변화에 직접적으로 작용하고, 이로 인해 행동 변화를 일으키는 글루탐산신경세포와 회백질연관성상세포의 전사도 유도하는 것으로 생각된다. 본 연구에서 5xFAD 알츠하이머병 모델 쥐에서 FTY720에 의한 행동 변화에 기여한 세포 소분류와 위치를 알 수 있었다. 5xFAD 알츠하이머병 모델 쥐에 FTY720에 의해 변한 공간 전사체는 정상 쥐에서의 공간 전사체와 유사한 패턴이었고, 이는 FTY720가 알츠하이머병의 치료제로서의 가능성을 보여줬다고 생각된다. 통합적인 전사체 분석은 향후 뇌를 표적으로 하는 약제의 공간적, 세포 특이적 효과를 평가하는 데에 적용 가능할 것으로 기대된다.

**주요어:** FTY720, 뇌, 약물 효과, 공간 전사체, 단일 세포 전사체, 세포 구성, 지역별 분포

**학번:** 2019 – 30531